Quaternary Geochronology 33 (2016) 61–75

Contents lists available at ScienceDirect

Quaternary Geochronology

journal homepage: www.elsevier.com/locate/quageo

Research paper

Clarifying the distal to proximal tephrochronology of the Millennium (B–Tm) eruption, Changbaishan Volcano, northeast China

Xuan-Yu Chen [a, b, c, d, *], Simon P.E. Blockley [b], Pavel E. Tarasov [e], Yi-Gang Xu [c], Danielle McLean [b, f], Emma L. Tomlinson [g], Paul G. Albert [f, h], Jia-Qi Liu [i], Stefanie Müller [e, j], Mayke Wagner [k], Martin A. Menzies [a, c]

[a] Department of Earth Sciences, Royal Holloway University of London, Egham, Surrey, TW20 0EX, UK
[b] Department of Geography, Royal Holloway University of London, Egham, Surrey, TW20 0EX, UK
[c] State Key Laboratory of Isotope Geochemistry, Guangzhou Institute of Geochemistry, Chinese Academy of Sciences, Guangzhou, 510640, China
[d] University of Chinese Academy of Sciences, Beijing, 100049, China
[e] Institute of Geological Sciences, Palaeontology, Free University Berlin, Malteserstr. 74–100, Building D, 12249, Berlin, Germany
[f] Research Laboratory for Archaeology and the History of Art, University of Oxford, Oxford, OX1 3QY, UK
[g] Department of Geology, Trinity College Dublin, Dublin 2, Ireland
[h] Department of Geography, Swansea University, Swansea, SA2 8PP, UK
[i] Key Laboratory of Cenozoic Geology and Environment, Institute of Geology and Geophysics, Chinese Academy of Sciences, Beijing, 100029, China
[j] Center for Ainu and Indigenous Studies, Hokkaido University, Kita 8, Nishi 6, Kita-ku, Sapporo, 060-0808, Japan
[k] Eurasia Department and Beijing Branch Office, German Archaeological Institute, Im Dol 2–6, 14195, Berlin, Germany

ARTICLE INFO

Article history:
Received 22 October 2015
Received in revised form
12 February 2016
Accepted 16 February 2016
Available online 18 February 2016

Keywords:
Changbaishan
Millennium eruption
B–Tm tephra
Lake Kushu
Cryptotephra
Tephrochronology
Radiocarbon
Bayesian age modelling

ABSTRACT

Tephra dispersed during the Millennium eruption (ME), Changbaishan Volcano, NE China provides one of the key stratigraphic links between Asia and Greenland for the synchronization of palaeoenvironmental records. However, controversy surrounds proximal-distal tephra correlations because (a) the proposed proximal correlatives of the distal ME tephra (i.e. B–Tm) lack an unequivocal chronostratigraphic context, and (b) the ME tephra deposits have not been chemically characterized for a full spectrum of element using grain-specific techniques. Here we present grain-specific glass chemistry, including for the first time, single grain trace element data, for a composite proximal sequence and a distal tephra from Lake Kushu, northern Japan (ca. 1100 km away from Changbaishan). We demonstrate a robust proximal-distal correlation and that the Kushu tephra is chemically associated with the ME/B–Tm. We propose that three of the proximal pyroclastic fall units were erupted as part of the ME. The radiocarbon chronology of the Kushu sedimentary record has been utilised to generate a Bayesian age-depth model, providing an age for the Kushu tephra which is consistent with high resolution ages determined for the eruption and therefore supports our geochemical correlation. Two further Bayesian age-depth models were independently constructed each incorporating one of two ice-core derived ages for the B–Tm tephra, providing Bayesian modelled ages of 933–949 and 944–947 cal AD (95.4%) for the Kushu tephra. The high resolution ice-core tephra ages imported into the deposition models help test and ultimately constrain the radiocarbon chronology in this interval of the Lake Kushu sedimentary record. The observed geochemical diversity between proximal and distal ME tephra deposits clearly evidences the interaction of two compositionally distinct magma batches during this caldera forming eruption.

1. Introduction

The Millennium eruption (ME) from the Changbaishan Volcano was a very large (VEI ≈ 7) eruption with the potential for ash dispersal across the Northern Hemisphere. Whilst the eruption was estimated to have had substantial volatile and sulfate aerosol emissions (Horn and Schmincke, 2000; Guo et al., 2002), it lacked a

* Corresponding author. Department of Earth Sciences, Royal Holloway University of London, Egham, Surrey, TW20 0EX, UK.
E-mail address: Xuanyu.Chen.2014@live.rhul.ac.uk (X.-Y. Chen).

http://dx.doi.org/10.1016/j.quageo.2016.02.003
1871-1014/

global impact on climate (Xu et al., 2013; Sun et al., 2014a). Distal products of the ME (i.e. B–Tm) have been reported in many localities including the Sea of Japan, the Japanese Archipelago (Machida and Arai, 1983; Furuta et al., 1986; Machida et al., 1990; Fukusawa et al., 1998; Nanayama et al., 2003; Kamite et al., 2010; Okuno et al., 2011; Hughes et al., 2013), northeast China (Sun et al., 2015) and the Greenland ice cores (Sun et al., 2014a) (Fig. 1a). As such it provides one of the potential key stratigraphic links between Asia and Greenland for the synchronization of palaeoenvironmental records. The proposed correlations between the distal ME tephra deposits and the Changbaishan Volcano (Machida et al., 1990; Sun et al., 2014a, 2015) require detailed chronostratigraphic studies and geochemical analyses of the proximal deposits and distal records. However, the proximal correlatives reported therein lack chronostratigraphic context and the ME tephra units have not been chemically characterized for a full spectrum of element using grain-specific techniques. Here we present the results of geochemical investigations of tephra units from proximal deposits with chronostratigraphic context, and a distal archive from Japan. This is then used to re-evaluate the proximal deposits, distal correlatives and the overall chronology for this eruption.

2. Background

2.1. Proximal volcanic deposits

The Changbaishan Volcano, situated on the border between China and North Korea (42°00′ N, 128°03′ E, Fig. 1a), is a polygenetic central stratovolcano with three main eruptive stages: early shield building, middle cone construction and a late explosive stage (Wei et al., 2007, 2013). During the latest explosive stage (<20 ka: Wei et al., 2013), a major caldera-forming eruption occurring at ~ AD 1000 (i.e. the "Millennium" eruption) produced a ca. 4.5 km wide caldera containing the crater lake called Tianchi (Machida et al., 1990).

The latest explosive stage recorded at Tianwen summit, on the Chinese flank of the crater contains four sequentially deposited pyroclastic fall units, C-4 [base], C-3, C-2 and C-1 [top], which are coloured yellow, light grey, dark grey and black, respectively (Fig. 1b). Stratigraphic and chronological studies of the Tianwen summit profile are summarized in Fig. 2. The lowermost C-4 yellow unit was dated by different methods and yielded ages around 4–5 ka (Liu et al., 1998; Wang et al., 2001; Yang et al., 2014). Hence, it

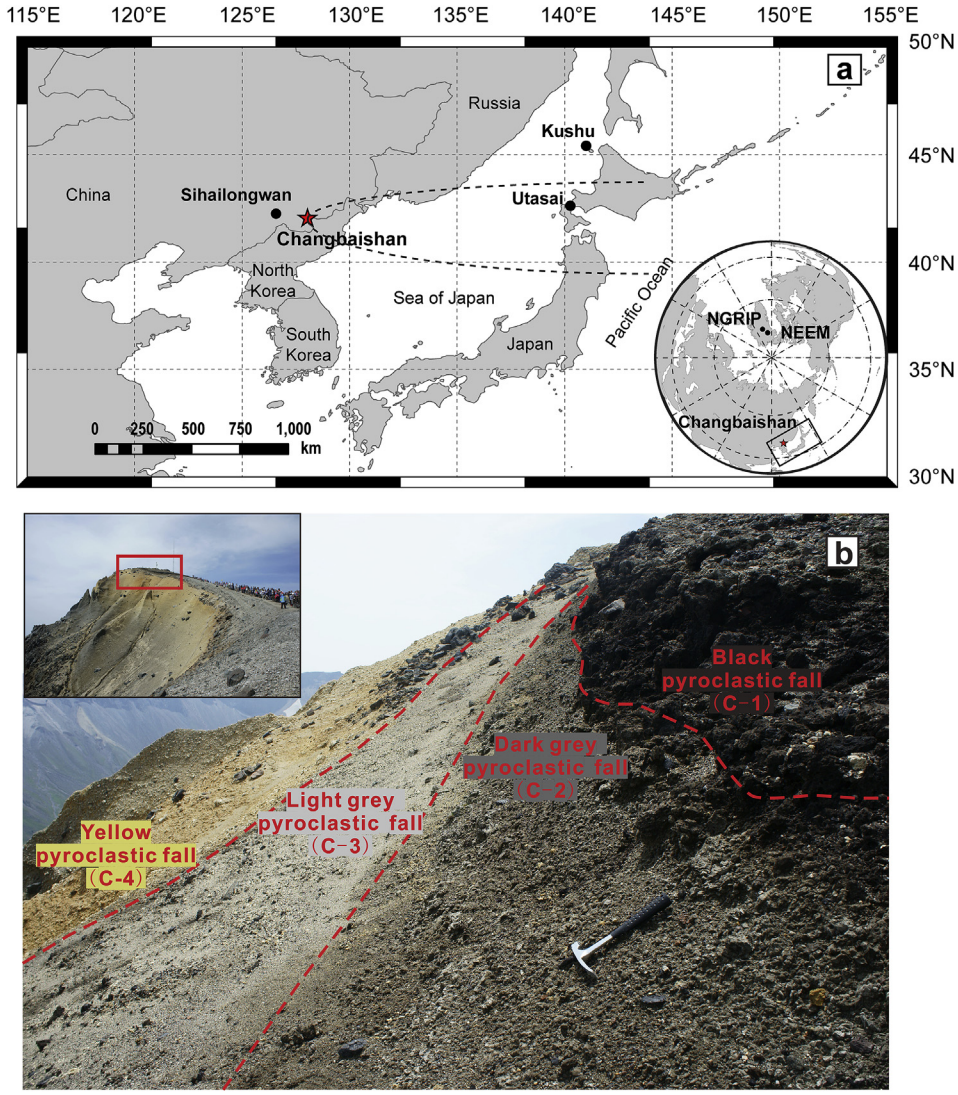

Fig. 1. (a) Location of the Changbaishan Volcano and the Lake Kushu distal archive on Rebun Island, northern Japan. The dashed line shows the previously reported distribution of B–Tm according to Machida and Arai (1983). Other occurrences of this tephra where the geochemical data used for comparison come from are marked on the map as well. (b) Sampled stratigraphy at the Tianwen summit on the Chinese flank of the Tianchi crater, Changbaishan Volcano, modified from Chen et al. (2014).

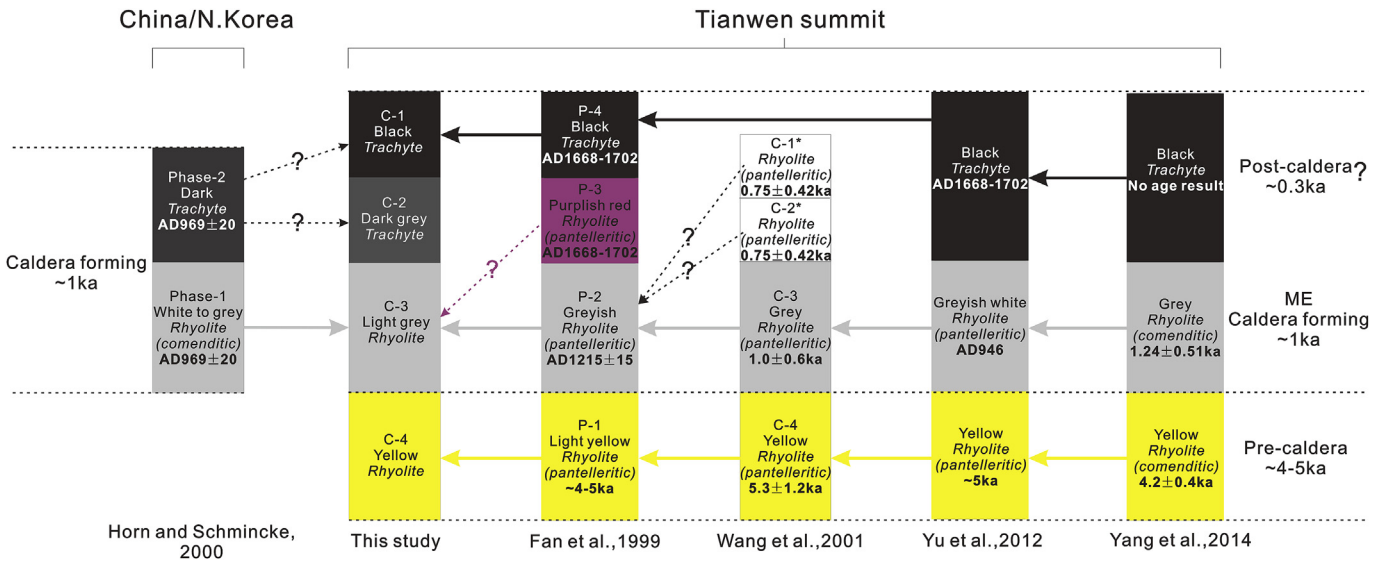

Fig. 2. Schematic illustration of previous stratigraphic and chronological studies of the Tianwen summit profile, Changbaishan Volcano. The solid arrows (black, grey, yellow) indicate correlations based on stratigraphy and the dashed arrows plus question mark indicate where correlations cannot be confirmed due to conflicting or inadequate stratigraphic information. Asterisks denote no colour description of tephra units and a question mark denotes uncertainty about the nature of an eruptive deposit. This paper focuses on the three upper pyroclastic fall units above the yellow pumice (i.e. light grey, dark grey and black units). (For interpretation of the references to colour in this figure caption, the reader is referred to the web version of this article.)

was believed to be the product of an older pre-caldera forming eruption (Fig. 2). The overlying C-3 light grey unit is a very widespread pyroclastic fall which covers the crater rim and extends eastwards for more than 15 km from the crater (Horn and Schmincke, 2000; Sun et al., 2014b). At the Tianwen summit profile, this light grey unit has been dated at ~1 ka by U-series TIMS (Wang et al., 2001) and $^{40}Ar/^{39}Ar$ (Yang et al., 2014) methods (Fig. 2). The same light grey-coloured tephra was visually identified in the environs of the volcano where extensive radiocarbon dating studies of charcoal samples confirmed that it has an age consistent with the onset of the last millennium (e.g. Horn and Schmincke, 2000; Nakamura et al., 2007; Yatsuzuka et al., 2010; Yin et al., 2012; Xu et al., 2013, Table 1). Therefore, the C-3 unit was regarded as the product of the ME. However, there is considerable controversy regarding the stratigraphic and chronological significance of the overlying C-2 and C-1 units. None of the previous studies reported a dark grey pyroclastic fall (here labelled C-2) overlying the C-3 light grey unit (Fig. 2). Fan et al. (1999) described a light purplish red welded tuff unit with a post-ME age overlying the light grey unit. This cannot be correlated to our C-2 unit on the basis of their colour and compositional discrepancies. Wang et al. (2001) mentioned two stratigraphically upper units without colour description, whose age and compositional information did not help to clarify the stratigraphic correlation. The two more recent stratigraphic and chronological studies, Yu et al. (2012) and Yang et al. (2014), both failed to identify the dark grey unit sitting in between the light grey and the uppermost black units. For the C-1 black pyroclastic fall, no age has yet been conclusively confirmed. By reviewing the historical records of "abnormal natural phenomenon", Cui et al. (1995) proposed three possible dates (i.e. AD 1668, 1702 and 1903) for the post-caldera eruptions of the Changbaishan Volcano. Ji et al. (1999) used thermo-luminescence (TL) to date the K-feldspar from the black pumice (C-1) and reported an age of 0.34 ± 0.03 ka. Based on these two pieces of

Table 1
Age results for the Millennium eruption from the dating of proximal and distal (B–Tm) tephra deposits.

Location	Method	Age	Ref.
Proximal			
Changbaishan environs (pyroclastic fall and flow deposits)	^{14}C wiggle-match dating	AD 940–952 (2σ)	Xu et al. (2013)
		AD 923–939 (2σ)	Yin et al. (2012)
		AD 945–960 (2σ)	Yatsuzuka et al. (2010)
		AD 930–943 (2σ)	Nakamura et al. (2007)
		AD 945–984 (2σ)	Horn and Schmincke (2000)
Tianwen summit (light grey fall)	$^{40}Ar/^{39}Ar$	1.24 ± 0.51 ka	Yang et al. (2014)
	U-series TIMS	1.0 ± 0.6 ka	Wang et al. (2001)
Distal			
Lake Kushu (Rebun, northern Japan)	Bayesian Modelling	AD 933–949 (2σ)	This study
		AD 944–947 (2σ)	
Greenland ice cores	Ice-core chronology	AD 946–947 (NS1-2011 timescale)	Sigl et al. (2015)
		AD 941 ± 1 (GICC05 timescale)	Sun et al. (2014a)
		AD 945 ± 4 (GISP2 timescale)	
Sihailongwan Maar Lake (NE China)	Varve chronology	AD 953 ± 37	Sun et al. (2015)
	Conventional ^{14}C	AD 940–1020 (2σ)	
Lake Ni-no-Megata/San-no-Megata (NE Japan)	Varve chronology	AD 929	Kamite et al. (2010)
Lake Ogawara (NE Japan)	Varve chronology	AD 937–938	Fukusawa et al. (1998)

evidence, Liu et al. (1999) concluded that the black unit (C-1) can be correlated to the AD 1668–1702 eruptive record. However, the "abnormal natural phenomenon" recorded by ancient people including "thunder" or "white ash rain" cannot be confidently and accurately attributed to a particular volcanic eruption. Moreover, the TL age from the black pumice cannot completely rule out the possibility that this C-1 unit could be an older eruptive, reset by a younger eruption. As such, the eruption age of the C-1 unit remains ambiguous and it could be either contemporaneous with the ME or post date the ME.

Controversy also surrounds geochemical studies of the proximal ME stratigraphy on the crater rim. Fan et al. (1999) and Yu et al. (2012) suggested that, at Tianwen summit, only the light grey unit (i.e. C-3) is the ME product and that it can be classified as pantelleritic rhyolite based on bulk rock chemistry (Fig. 2). However, Horn and Schmincke (2000) argued that the ME deposits should have included two phases: a major rhyolitic phase producing white to grey coloured pumice, and a minor later phase forming trachytic agglutinates mantling the inner crater walls. Meanwhile, their electron microprobe glass data indicated that the widespread light grey pumice has a peralkalic composition akin to comendite rather than pantellerite (Fig. 2). More recently, Sun et al. (2014a) reported major element glass chemistry for tephras sampled from the Korean side, indicating that the proximal ME deposits have bimodal compositions (i.e. trachyte and rhyolite). Although they described the outcrop containing white-yellow, grey and black pyroclastic fall, it is not easy to correlate this sequence to the Tianwen summit profile because no detailed stratigraphic context was provided.

2.2. Distal B–Tm records and the proximal correlatives

The B–Tm tephra, which was named after its source volcano Baegdusan (i.e. Changbaishan Volcano) and its type locality in Tomakomai, Hokkaido, was first reported to be found in the Sea of Japan and Hokkaido and the northern part of Honshu (Machida and Arai, 1983). It was suggested to be the distal equivalent of the ME on the basis of its composition and stratigraphic position (i.e. relative age), as well as petrographic features (Machida et al., 1990). Later on, the B–Tm tephra was reported in many localities across northeast Asia and in the Greenland ice cores (Furuta et al., 1986; Fukusawa et al., 1998; Nanayama et al., 2003; Kamite et al., 2010; Okuno et al., 2011; Hughes et al., 2013; Sun et al., 2014a, 2015). However, few of the above-mentioned studies have focused on the distal-proximal tephra correlation and the proposed proximal correlatives lack either independent dating to corroborate their "millennium" age (e.g. Machida et al., 1990) or unequivocal stratigraphic context (e.g. Sun et al., 2014a, 2015). As such hardly any clearly described outcrops have been reliably confirmed as the proximal equivalent, which leaves the B–Tm tephra almost distally described only. Moreover, the identification, characterization and correlation of the B–Tm is typically based on major element glass chemistry. Whilst there are some effective major element discriminants that can be used to separate contemporaneous marker tephras (Sun et al., 2014a), one has to be careful because volcanoes can produce eruptions with similar compositions over a considerable time window (e.g. Smith et al., 2011a, c; Lane et al., 2012; MacLeod et al., 2015). Hence we highly recommend that a full spectrum of major, minor and trace elements should be applied when correlating tephras as this greatly increases the reliability of the resultant correlations. Since the abundances of trace elements are more sensitive to magmatic processes, they are widely used to secure tephra correlations (e.g. Allan et al., 2008; Smith et al., 2011a; Tomlinson et al., 2012; Lane et al., 2012; Albert et al., 2012, 2013; Tomlinson et al., 2014; Albert et al., 2015; Tomlinson et al., 2015; Lane et al., 2015).

3. Sampling

3.1. Changbaishan tephra

Proximal fall lapilli samples from the C-1, C-2 and C-3 units were collected at the Tianwen summit (42°01′33″ N, 128°04′00″ E) under tight stratigraphic control. Sub-samples of the light grey pumice from Yang et al. (2014) are included in our C-3 sample set as they were collected from the same profile and the same unit, and were dated by $^{40}Ar/^{39}Ar$ to corroborate the millennium age. Lapilli sized samples were crushed, cleaned, dried and clean fragments were examined and picked under the microscope then mounted in epoxy resin for geochemical micro-beam analysis. The samples from these three fall units contain alkali feldspar as the dominant phenocryst phase, with some minor contributions of olivine, pyroxene and quartz. The C-1 unit contains the highest percentage of phenocryst among all the three units. SEM images were taken to reveal the vesicularity and the location of phenocrysts prior to micro-beam analysis (Fig. 3). SEM images show that the C-3 pumice samples are made up of both highly vesiculated and less vesiculated glasses (Fig. 3a–b), with some highly vesiculated glasses being very stretched (Fig. 3a). The vesicularity of the C-3 sample was estimated to be ~60% (Yu et al., 2012). The C-2 pumice samples contain highly vesiculated glasses (Fig. 3c) and have a similar level of vesicularity with the C-3 samples. The C-1 pumice samples mainly contain poorly vesiculated glasses (Fig. 3d), with the mount of vesicles decreasing significantly relative to the C-2 and C-3 samples. The vesicularity of C-1 sample was estimated to be less than 50% (Yu et al., 2012), which is consistent with the observation that the C-1 samples are slightly welded whereas the C-2 and C-3 samples are not.

3.2. Lake Kushu tephra

Lake Kushu (45°25′55″ N, 141°02′13″ E), ca. 1100 km away from the Changbaishan Volcano, is the only fresh-water lake of Rebun Island in the Sea of Japan, northwest off Hokkaido (Fig. 1a). Located in the northern part of the island, about 230–400 m from the coast, the lake has a kidney bean shape and a maximum length of ca. 1100 m. The maximum water depth reaches ca. 6 m in the eastern part of the lake with average depths of about 3–5 m. The bottom sediment of Lake Kushu has been considered as a valuable natural archive which stores detailed, high-resolution information about post-glacial environmental changes (Kumano et al., 1990). Therefore, Lake Kushu has been selected as one of the key study sites in the Baikal-Hokkaido Archaeology Project (BHAP), aiming to fill the existing gap in the current knowledge and to address the role of climate and environmental change in the life of northern hunter-gatherers (Weber et al., 2013). In February 2012, two parallel sediment cores (RK12-01 and RK12-02) were collected in the central part of the lake from the thick ice cover. The recovered composite core (RK12) revealed a continuous, partly laminated, organic-rich ca. 19.5 m long sediment column. The RK12 core age model built upon the 57 calibrated AMS radiocarbon dates suggests that the sedimentation continued over the past ca. 17,000 years (Müller et al., in press).

This lake was also selected for visible tephra and cryptotephra analyses due to the potential for tephras to be located from Japanese, Korean and Chinese volcanoes, and coupled with the high precision radiocarbon chronology and palaeoenvironmental record. The tephra study covered the entire core archive, although here we focus only on the tephra of approximate millennium age, based on the radiocarbon chronology. A detailed

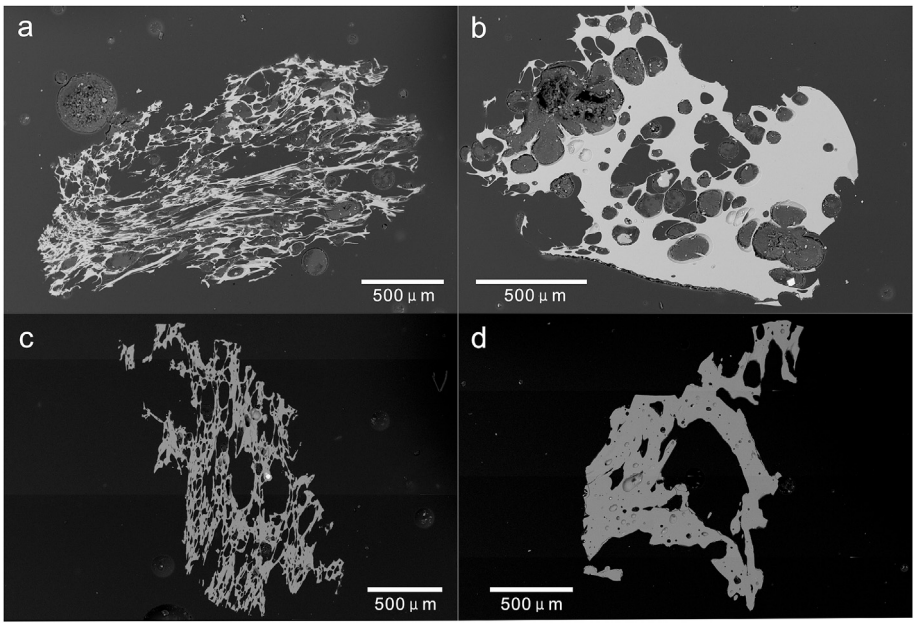

Fig. 3. SEM images of the proximal Changbaishan tephras. (a–b) the C-3 light grey pumice, both highly vesiculated and less vesiculated glasses with some highly vesiculated glasses being strongly stretched; (c) the C-2 dark grey pumice, vesicular and stretched glasses; (d) the C-1 black pumice samples that have the highest content of phenocryst and the least vesicularity among all the three proximal fall units.

tephrochronological study of the whole core is currently in preparation (Chen et al., in progress). Distal tephras were separated using procedures outlined by Blockley et al. (2005). The extracted glass shards were mounted in Canada Balsam on glass slides and examined using an Olympus CX-41 microscope fitted with cross-polarising filters. In order to identify the location of each discrete tephra layer, two steps of sub-sampling on the core materials were carried out. In the first scanning phase, 20 cm sampling interval was used to produce the range-finder counts that revealed the quantitative distribution of shards per gram of dry sediment for the complete composite core. A detailed analysis phase termed point-sample count, with 1 or 2 cm sampling interval, was undertaken later to locate the precise depth of the tephra where range-finders showed high concentration of glass shards. The point-sample counts relative to this research clearly show that the initial onset of the tephra input appears at the composite depth of 152–151 cm whilst the peak of it sits at 151–150 cm (Fig. 4). No visible ash layer was identified at these depths during core opening and sediment description though the tephra counts show quite large numbers. Individual shards (Fig. 5) were picked in the interval of 150–152 cm and embedded in resin, sectioned and polished ready for geochemical analysis.

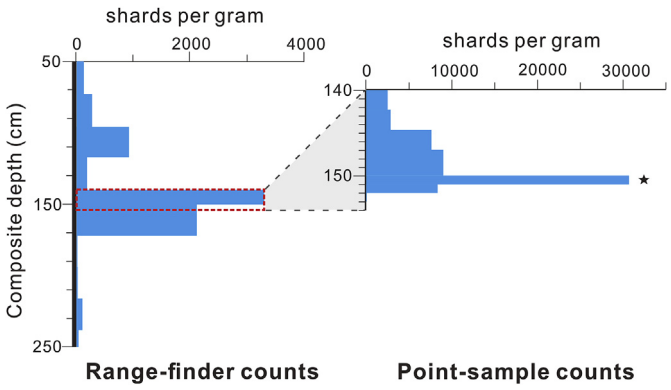

Fig. 4. Tephra shard concentrations measured in sediments in the top 2 m of samples from Lake Kushu. Shard counts are given as numbers of shards per gram of dry sediment. The star marks the peak of the tephra input.

4. Analytical methods

4.1. Electron micro-probe analysis (EMPA)

Major and minor element concentrations of glasses of proximal pumices and distal tephra shards were determined using Jeol JXA-8600 wavelength-dispersive electron microprobe (WDS-EMPA), equipped with 4 spectrometers and SamX software, at the Research Laboratory for Archaeology and the History of Art, University of Oxford. An accelerating voltage of 15 kV, low beam current (6 nA), and defocused (10 μm) beam were used to minimize Na migration. Count times were 30 s for Si, Al, Mg, Ti, Ca, K and Fe on each peak. Na was analysed for 12 s, Cl and Mn for 50 s and P for 60 s on each peak. The instrument was calibrated for each set of beam conditions using a suite of appropriate mineral standards. The calibration was verified using a range of secondary glass standards (MPI-DING suite) including the ATHO-G (rhyolite), StHs6/80-G (andesite) and GOR132-G (komatiite) glasses from the Max Planck Institute (Jochum et al., 2006). Samples with analytical totals <94% were discarded. All the analyses presented in the text, plots and tables are normalised to 100 wt.% for comparative purposes. Analytical precision is typically <0.8% relative standard deviation (RSD) for Si; <5% RSD for analytes with concentrations >0.8 wt.% with the exception of Na (7–10%). All standard data is presented in the supplementary material.

4.2. Laser ablation inductively coupled plasma mass spectrometry (LA-ICP-MS)

Trace element analyses of glasses of proximal and distal tephras were performed using a Thermo Scientific iCAP Q ICP-MS coupled to an Analyte Excite excimer laser-ablation system at the

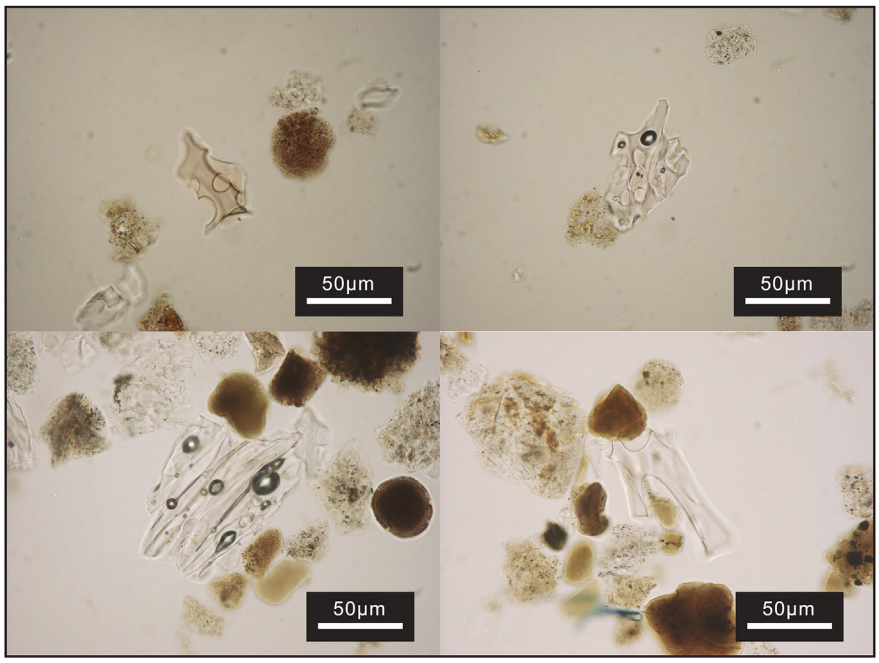

Fig. 5. Light microscope photographs of tephra shards extracted from Lake Kushu sediments at 150–152 cm composite depth.

Department of Geology, Trinity College Dublin. Spot sizes of 18, 24, 30 and 36 μm were used, depending on the size of the area available for analysis in different samples. The repetition rate was 5 Hz and the count time was 40 s (200 pulses) on the sample and 40 s on the gas blank (background). The ablated sample was transported in He gas flow (0.65 L min^{-1}) with additional N_2 (5 ml min^{-1}) via a signal smoothing device. Concentrations were calibrated using NIST612 with ^{29}Si as the internal standard. Data reduction was performed manually using Microsoft Excel that allowed removal of portions of the signal compromised by the microcryst, void or resin component. Full details of the analytical and data reduction methods are described in Tomlinson et al. (2010). Accuracies of ATHO-G and StHs6/80-G MPI-DING glass analyses are typically <5% for most elements, <10% for Y, Zr, Nb, Gd and <15% for Ta. Reproducibility of ATHO-G analyses is <5% RSD for all trace elements with the exception of U (<7%).

5. Results

Glasses from juvenile clasts found in both proximal and distal deposits have compositions ranging from trachyte to rhyolite, with the rhyolitic population straddling the alkaline-subalkaline boundary (Fig. 6a). On a molecular basis, all the rhyolitic glasses and the majority of trachytic glasses reported herein have $(Na_2O + K_2O) > Al_2O_3$, whereas only few trachytic glasses show subtle $(Na_2O + K_2O) \leq Al_2O_3$. By definition, they are peralkaline trachyte and rhyolite. According to the classificatory scheme for peralkaline extrusive rocks (MacDonald, 1974), they can be further classified as comenditic trachyte and comendite, respectively (Fig. 6b). Representative major, minor and trace element glass compositions of proximal pumices and distal shards are given in Table 2. The full geochemical data sets are presented in the supplementary material.

5.1. Glass chemistry of proximal deposits

5.1.1. C-1 fall deposits

The uppermost C-1 fall unit at Tianwen summit has a comenditic trachyte glass composition (Fig. 6b). The glasses are characterized by low CaO (1.1–1.5 wt.%) and MgO (0.1–0.3 wt.%), high K_2O (4.8–6.2 wt.%) and significantly high FeO_t (4.3–5.1 wt.%) with homogeneous SiO_2 (64.7–66.6 wt.%; Fig. 7a–d). They show an overall trend of decreasing total alkalis with increasing SiO_2 (Fig. 6a). Trace element data reveal that these glasses have limited compositional variations with 9–16 ppm Th, 14–40 ppm Ba, 3–5 ppm Ta, 49–73 ppm Nd and 30–45 ppm Y. They form compositional clusters in most of the trace element bi-plots (Fig. 7f–h). C-1 glasses have light rare earth element (LREE) enrichment relative to the heavy rare earth element (HREE) with La/Yb ratios ranging from 21 to 25. Mantle-normalised spider diagram reveals that C-1 glasses are up to more than 200 times more enriched than the primitive mantle (Fig. 8). They are characterized by pronounced negative anomalies in Ba, Sr and Eu in response to the fractionation of K-feldspar, which is a dominant phenocryst phase in the juvenile clasts.

5.1.2. C-2 fall deposits

There is significant overlap in glass compositions of the C-2 fall unit and the overlaying C-1 unit. The C-2 glasses are also classified as comenditic trachyte (Fig. 6b). They extend to slightly more evolved SiO_2 (65.4–67.7 wt.%), have less variable K_2O (5.5–6.1 wt.%), comparable CaO (1.0–1.4 wt.%), FeO_t (4.4–5.2 wt.%) and MgO (0.1–0.3 wt.%) relative to those of the C-1 glasses (Fig. 7a–d). The compositional similarity between the two units can also be seen in the trace element data. C-2 glasses show trace element concentrations of 12–19 ppm Th, 14–39 ppm Ba, 4–6 ppm Ta, 61–78 ppm Nd, and 36–51 ppm Y, which form almost identical compositional clusters overlapping the C-1 glasses (Fig. 7e–h). Mantle-normalised spider diagram reveals that the multi-element profiles of C-2 glasses have similar distribution pattern and incompatible element enrichment level with those of the C-1 glasses (Fig. 8). Nevertheless, some subtle differences in composition can be observed: (1) C-1 glasses have some least evolved components that are not seen in C-2 deposits (e.g. lower SiO_2 content and lower incompatible element enrichment level; Figs. 6a and 8); (2) C-2 glasses extend to more evolved compositions than

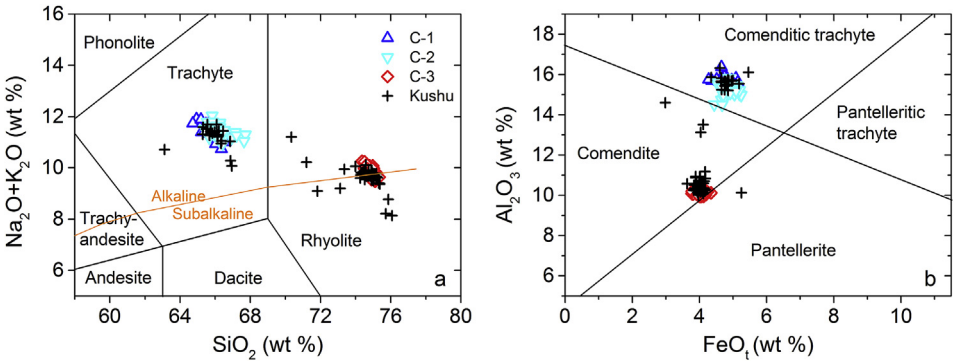

Fig. 6. (a) TAS classification (Le Bas et al., 1986) diagram showing the glass compositions of proximal fall deposits (i.e. C-1, C-2 and C-3) and distal Kushu tephra. The boundary separating the alkaline and subalkaline series is from Irvine and Baragar (1971). (b) Classificatory diagram for peralkaline extrusive rocks (MacDonald, 1974) showing the glasses compositions of the peralkaline proximal and distal tephras.

Table 2
Representative major, minor and trace element data for glasses from proximal volcanic deposits at Tianwen summit and distal Kushu tephra. Full geochemical data sets are available in the Supplementary material file.

Locality	Tianwen summit							Lake Kushu					
Unit/group	C-3			C-2		C-1		Rhyolite			Trachyte		
Sample	10CB-2-1	14-1-1	14-1-4	14-5-1	14-5-9	14-4-1	14-4-5	RH490-20	RH555-33	RH554-37	RH555-30	RH554-6	Rh554-8
Material	Pumice							Tephra shard					
Major elements wt.%													
SiO_2	74.98	74.73	74.93	66.06	66.42	66.08	66.24	74.90	74.97	70.34	66.15	66.12	66.20
TiO_2	0.21	0.23	0.19	0.41	0.52	0.45	0.44	0.24	0.20	0.30	0.48	0.48	0.42
Al_2O_3	10.06	10.15	10.23	15.37	15.26	15.69	15.09	10.58	10.36	14.60	15.49	15.66	15.86
FeO_t	4.15	4.23	4.08	4.96	4.91	4.37	4.92	3.92	4.13	2.98	4.81	4.64	4.35
MnO	0.13	0.10	0.02	0.13	0.12	0.08	0.20	0.10	0.08	0.09	0.17	0.16	0.12
MgO	0.00	0.04	0.00	0.19	0.17	0.22	0.17	0.00	0.00	0.00	0.23	0.18	0.17
CaO	0.20	0.16	0.21	1.25	1.30	1.25	1.23	0.23	0.23	0.19	1.25	1.26	1.26
Na_2O	5.12	5.45	5.26	5.68	5.54	6.06	5.90	5.27	5.25	6.05	5.45	5.67	5.81
K_2O	4.51	4.27	4.50	5.76	5.57	5.58	5.65	4.26	4.30	5.16	5.76	5.62	5.63
P_2O_5	0.01	0.02	0.00	0.04	0.06	0.09	0.04	0.00	0.00	0.03	0.06	0.07	0.05
Cl	0.63	0.62	0.57	0.15	0.13	0.14	0.12	0.51	0.48	0.25	0.15	0.14	0.13
Analytical total	98.02	99.61	98.08	99.29	98.47	98.13	99.89	97.02	97.97	98.60	98.98	98.26	99.19
$K_2O + Na_2O$	9.63	9.72	9.76	11.44	11.11	11.64	11.55	9.53	9.55	11.21	11.21	11.29	11.44
Trace elements ppm													
Rb	419	426	428	153	157	143	143	417	403	308	143	157	150
Sr	2.7	3.0	6.1	6.3	5.9	8.4	6.8	2.8	2.7	2.7	6.6	10.6	8.6
Y	125	143	156	43	43	37	42	144	130	66	37	48	38
Zr	2152	2377	2305	655	682	564	653	2395	2252	1260	589	792	585
Nb	280	302	299	93	95	79	88	303	286	195	84	107	87
Ba	7.7	9.1	9.9	19.2	17.6	28.6	19.9	8.5	9.7	10.8	19.9	31.0	30.1
La	135	152	173	89	92	77	87	163	148	127	82	101	79
Ce	288	316	336	175	175	154	170	328	307	246	159	197	155
Pr	31.8	35.4	39.6	19.0	19.1	16.5	18.3	34.7	33.2	23.6	17.2	20.6	17.7
Nd	118	130	149	71	71	62	69	136	123	78	63	77	61
Sm	26.0	29.3	32.2	13.4	14.3	11.7	13.0	31.6	26.6	16.5	12.1	14.3	13.1
Eu	<LOD	0.4	<LOD	<LOD	<LOD	0.4	0.4	0.4	<LOD	<LOD	<LOD	<LOD	<LOD
Gd	23.9	27.2	29.3	10.3	10.5	9.6	10.1	27.4	23.0	13.3	9.3	11.4	9.1
Dy	23.3	28.2	29.7	9.1	9.3	7.8	8.7	25.9	24.0	12.6	7.7	9.7	8.0
Er	12.9	14.4	15.0	4.6	4.5	3.8	4.2	13.7	11.9	7.3	4.1	5.0	4.0
Yb	10.7	12.7	12.9	4.0	4.1	3.5	4.0	11.9	10.7	5.9	3.5	4.9	3.6
Hf	52.2	60.9	56.7	16.2	16.2	13.2	15.1	58.1	51.3	30.3	13.9	18.2	13.9
Ta	15.9	17.1	17.0	4.7	4.8	4.0	4.5	15.4	14.3	9.7	4.0	5.4	4.1
Th	48.9	56.8	52.4	15.1	15.2	12.4	14.5	52.9	46.1	30.1	12.9	17.7	13.4
U	11.4	12.7	12.8	3.4	3.4	2.8	3.0	11.5	10.7	7.0	2.7	3.7	3.0

C-1 glasses (e.g. higher SiO_2 content and higher incompatible element enrichment level; Figs. 6a and 8).

5.1.3. C-3 fall deposits

Glasses of the lower C-3 fall unit have a composition straddling the boundary between alkaline and subalkaline rhyolite (Fig. 6a) and can be specifically classified as comendite (Fig. 6b). C-3 glasses are highly homogeneous with restricted major element compositional ranges. They have concentrations of highly evolved SiO_2 (74.4–75.3 wt.%) with lower CaO (0.1–0.3 wt.%), MgO (<0.1 wt.%), K_2O (4.3–4.6 wt.%) and FeO_t (3.8–4.3 wt.%) than those of the overlying trachytic units (i.e. C-1 and C-2; Fig. 7a–d). Trace element concentration data for C-3 glasses form linear clusters in element bi-plots (Fig. 7e–h). They have higher contents of Th (44–57 ppm), Ta (14–18 ppm), Nd (111–149 ppm), Y (117–156 ppm) and lower Ba (7–10 ppm) relative to the upper

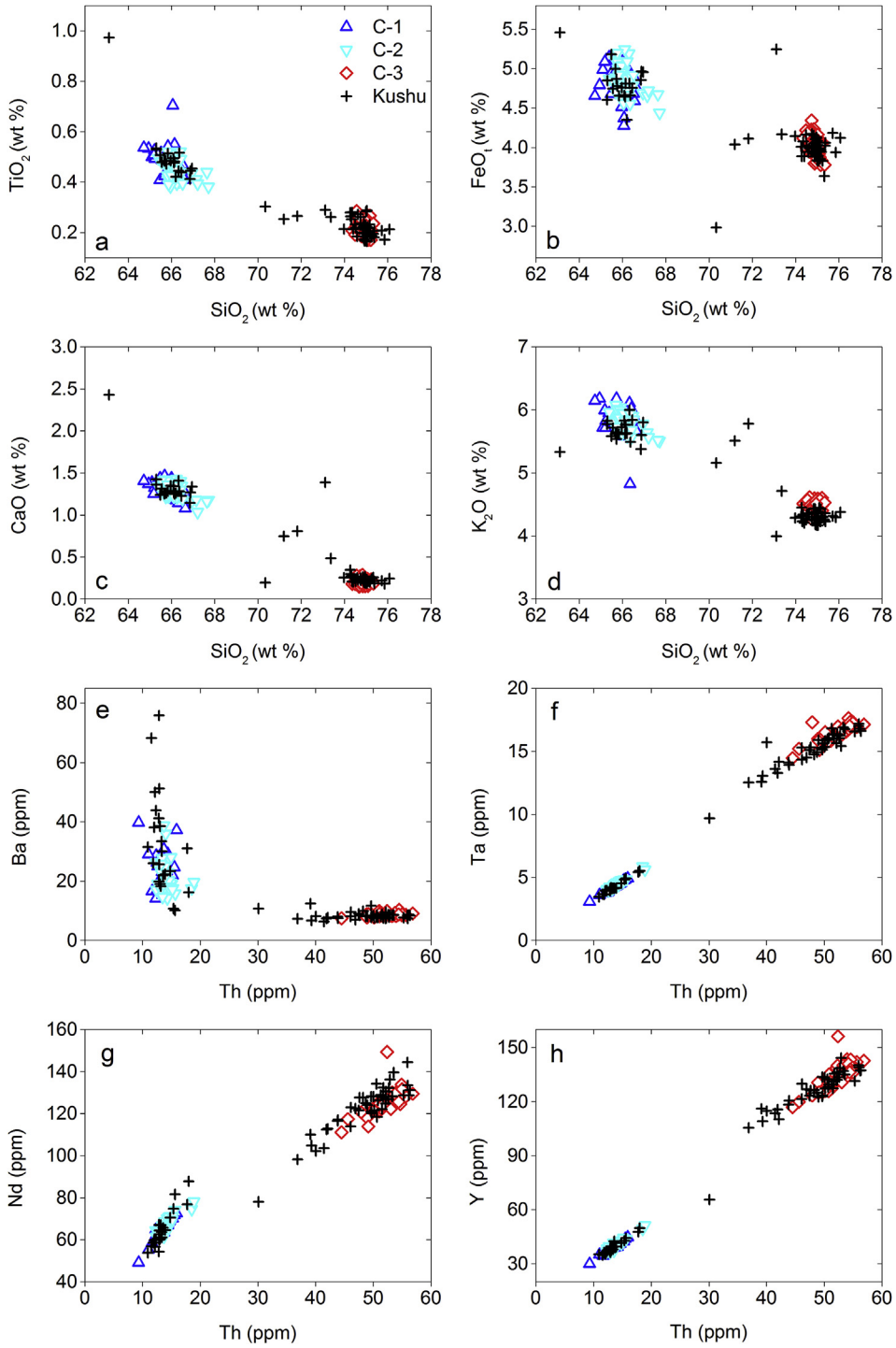

Fig. 7. Major and trace element variation diagrams showing the glass compositions of proximal fall deposits and distal Kushu tephra.

trachyte units (Fig. 7e–h). C-3 glasses show LREE enrichment relative to the HREE with a lower LREE/HREE fractionation level (La/Yb = 11–13) than those of the trachytic glasses. Mantle-normalised spider diagram shows that the C-3 glasses are up to more than 600 times more enriched than the primitive mantle, with more pronounced depletions in Ba, Sr and Eu relative to the trachytic units (Fig. 8). It is worth noting that, in their multi-element profiles, the trachytic glasses and the C-3 rhyolitic glasses show different trends in anomalies of Nb–Ta (Fig. 8).

5.2. Glass chemistry of distal tephra

The distal tephra found in Lake Kushu shows significant heterogeneity with compositions ranging from trachyte to rhyolite (Fig. 6a). This can be further classified as comenditic trachyte and comendite respectively (Fig. 6b). The less evolved trachytic components are characterized by relatively homogeneous SiO_2 (typically between 65.3 and 67.0 wt.%), low CaO (typically between 1.1 and 1.4 wt.%) and MgO (typically between 0.1 and 0.3 wt.%), high

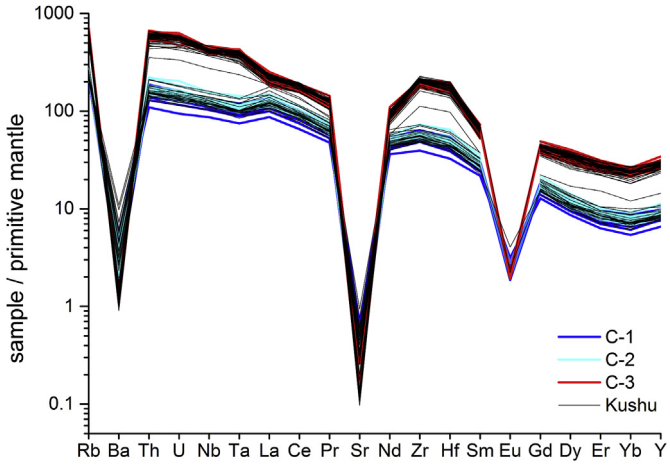

Fig. 8. Primitive mantle normalised trace element compositions of glasses from proximal fall deposits and distal Kushu tephra. Primitive mantle values are from Sun and McDonough (1989).

K_2O (5.3–6.0 wt.%) and FeO_t (4.4–5.5 wt.%), while the more evolved rhyolitic shards have heterogeneous SiO_2 (70.3–76.1 wt.%), lower CaO (typically <0.8 wt.%), MgO (<0.1 wt.%), K_2O (typically <4.7 wt.%) and FeO_t (typically < 4.2wt.%; Fig. 7a–d). The two populations collectively show an overall trend of decreasing TiO_2, CaO, MgO, FeO_t and K_2O (Fig. 7a–d) with increasing SiO_2, while the Na_2O contents between the trachyte and rhyolite remain fairly constant (4.3–6.0 wt.% and 3.3–6.0 wt.% respectively).

Mantle-normalised spider diagram shows that the distal trachytic and rhyolitic glasses are comparable in incompatible element distribution patterns and enrichment levels to the proximal trachytic and rhyolitic glasses respectively (Fig. 8). All the distal glasses show LREE enrichment relative to HREE and pronounced negative anomalies in Ba, Sr and Eu (Fig. 8). Nevertheless, the less evolved trachytic glasses show more pronounced fractionation of LREE/HREE (La/Yb = 21–29) and less significant Ba, Sr and Eu anomalies relative to the highly evolved rhyolitic glasses (La/Yb typically <15). The two compositional groups clearly define two evolutionary trends in most of the trace element bi-plots (Fig. 7e–h). The trachytic glasses have trace element variations with 11–18 ppm Th, 10–76 ppm Ba, 4–6 ppm Ta, 54–88 ppm Nd and 37–50 ppm Y, while the rhyolitic glasses show significantly higher contents of Th (30–56 ppm), Ta (10–17 ppm), Nd (78–144 ppm), Y (66–144 ppm) and lower Ba (6–12 ppm; Fig. 7e–h). The rhyolitic glasses contain an analysis that is characterized by noticeably lower concentrations in most of the measured trace elements (Th = 30 ppm, see Table 2: RH554-37) and higher La/Yb ratio (La/Yb = 22) than any other rhyolite. Nevertheless, this analysis lies on the evolutionary trend of the rhyolitic members (Fig. 7g).

6. Interpretation

6.1. Proximal-distal glass correlation

Proximal-distal relationships are assessed in this section based on the glass geochemistry presented above. Overall, glass shards found in Lake Kushu are highly heterogeneous and broadly overlap all three proximal fall units at a major, minor and trace element level (Figs. 7 and 8).

The two proximal trachytic units, C-1 and C-2, share broadly overlapping major, minor and trace element glass chemistries, which makes it problematic to distinguish between these two units based on glass chemistry alone. The trachytic glasses of the distal Kushu tephra overlap with the two proximal trachytic units (Figs. 7 and 8). Subtle differences can be recognized between the proximal and distal trachytic glasses: (1) Kushu trachytic glasses have a least evolved composition that is not seen in proximal trachytic glasses (Fig. 7a); (2) Kushu trachytic glasses have greater compositional variations of highly depleted trace element (e.g. Ba and Sr) than proximal trachytic glasses (Fig. 7e), which might be affected by analysis of microlite of distal shards in LA-ICP-MS.

The proximal rhyolitic unit C-3 geochemically overlaps the most evolved compositions of the distal rhyolitic glasses. These most evolved distal compositions ($SiO_2 \geq 74.0$ wt.%, n = 41) make up the majority of the Kushu rhyolitic glasses (n = 46) and could not be separated from the C-3 glasses in the major or trace element bi-plots (Fig. 7). The mantle-normalised spider diagram corroborates the geochemical overlaps at a full spectrum of element level (Fig. 8). Nevertheless, Kushu rhyolitic glasses have some less fractionated compositions that are not seen in the C-3 glasses (Fig. 6a).

In summary, the distal Kushu tephra shows compositional heterogeneity and a continuum of compositions ranging from trachyte to rhyolite. The three proximal fall units collectively comprise compositionally identical trachyte and rhyolite but without the intervening compositional continuum. Given the similarity between the trachyte and rhyolite end-members we propose a correlation between the distal Kushu tephra and all three of the investigated proximal units.

6.2. Comparison with the published data

In order to determine the provenance of the tephras reported herein and to investigate the geochemical diversity between the well-correlated proximal and distal tephras, we compare our glass chemistries with those of the published proximal ME tephra and B–Tm, along with other widespread late Quaternary marker tephras in and around the Northeast Asia area. Since all the available data are major element glass chemistry, comparison can only be made at a major element level.

Major element glass chemistry provides some basic discriminants for the identification of the B–Tm tephra. The B–Tm tephra has distinctive compositional heterogeneity ranging from trachyte to alkaline/subalkaline rhyolite with a fairly high total alkali content (8–12 wt.%; Fig. 9a). However, the late Quaternary Kyushu tephra layers (e.g. K-Ah, AT, Aso-4 and Ata) and Holocene Kamchatka tephra deposits typically plot into the subalkaline area, and the early Holocene Ulleungdo tephra (i.e. U-Oki) straddles the boundary between phonolite and trachyte (Fig. 9a). The B–Tm tephra has lower CaO than that of the Kyushu and Kamchatka tephras in a given SiO_2, and higher SiO_2 than that of the Ulleungdo tephra (Fig. 9b). The FeO_t vs. CaO bi-plot is an excellent discriminant (Fig. 9c) since the B–Tm tephra has a fairly high FeO_t content (typically between 3.8 and 5.6 wt.%) coupled with a relatively low CaO content (typically <1.5 wt.%), given its highly evolved composition ($SiO_2 > 63$ wt.%). All the proximal and distal tephras reported herein show major element compositions that correspond precisely to the published B–Tm chemistries, and can be separated from tephras from other volcanic settings in the same region (Fig. 9). On this basis we conclude that all our proximal and distal tephra deposits are the product of the ME.

Sun et al. (2014a) reported the major element glass chemistry for a proximal ME sequence in North Korea which included the white-yellow, grey and black fall pumices. The major element chemistry for glasses from this ME sequence reveals an overlap with the proximal units described herein (Fig. 10a–b), suggesting both sequences relate to the ME. Most importantly, the proximal ME tephra units at Chinese and Korean sequences on the crater rim are both characterized by significant geochemical bimodality (i.e.

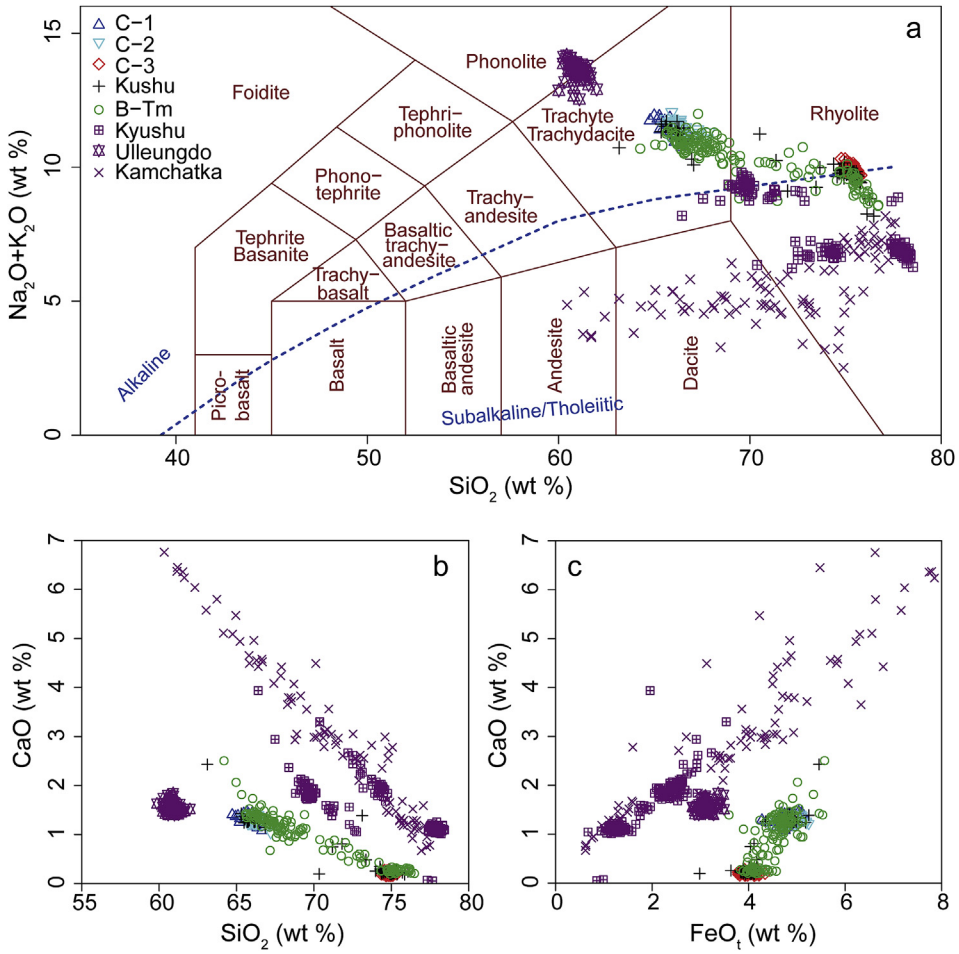

Fig. 9. (a) TAS classification (Le Bas et al., 1986) diagram and (b–c) major element variation diagrams showing the glass compositions of tephras reported herein along with the published data for comparison. The published data are glass compositions of the B–Tm and the widespread late Quaternary tephras from other volcanic settings in the Northeast Asia area. B–Tm includes the reported distal ME tephra deposits found in northeast China (Sun et al., 2015), Sea of Japan (Machida et al., 1990), Hokkaido (Hughes et al., 2013) and Greenland (Coulter et al., 2012; Sun et al., 2014a). Kyushu represents late Quaternary tephras (e.g. K-Ah, AT, Aso-4 and Ata) from volcanoes in Kyushu Island, Japan (Smith et al., 2013). Ulleungdo represents the early Holocene U-Oki tephra erupted from Ulleungdo, South Korea (Smith et al., 2011b). Kamchatka represents the tephra layers from major Holocene eruptions in Kamchatka Peninsula, Russia (Kyle et al., 2011).

trachyte and rhyolite) with no composition continuum plotting in the range of 69–74 wt.% of SiO_2 (Fig. 10a–b). This is in contrast to the B–Tm glass chemistries. The mid-range to distal ME tephra layers found in the Sihailongwan Lake (NE China; Sun et al., 2015), Sea of Japan (Machida et al., 1990), Utasai Bog (Hokkaido; Hughes et al., 2013) and Lake Kushu (Rebun, this study) reveal continuous compositions with data plotting in the compositional gap between the end-member compositions defined by proximal samples (Fig. 10c–d). Interestingly, although the ultra-distal B–Tm tephra deposits found in the Greenland ice cores contain very few shards (Coulter et al., 2012; Sun et al., 2014a), their compositions plot within the proximal compositional gap (Fig. 10c–d). Overall the proximal fall units deposited on the crater rim only preserve bimodal compositions for the caldera forming eruption, whereas the mid-range to distal tephra layers preserve a complete compositional range including the bimodal end-member compositions and intermediate compositions.

7. Discussion

7.1. Proximal-distal expression of the ME

As in the case of B–Tm tephra deposits reported from other localities, the single distal tephra layer found in Lake Kushu has compositional variation ranging from trachyte to rhyolite. This indicates the magmatic system that produced this distal ME tephra must have had the same compositional heterogeneity. In contrast the proximal C-3 unit is characterized by homogeneous rhyolite without any trachytic component. As such the C-3 unit alone cannot be the proximal equivalent of the B–Tm, though it is the most widespread unit in the Changbaishan volcanic region (Horn and Schmincke, 2000). Our glass chemistry shows that the geochemical bimodality observed between the proximal units C-3 to C-1 is comparable to the end-member compositions of the distal Kushu tephra. Importantly there is major, minor and trace element geochemical overlap between the proximal and distal end-member compositions which significantly increases the reliability of the tephra correlation. Hence, we propose that the proximal record of the ME at Tianwen summit is a composite sequence that includes the light grey, dark grey and black (i.e. C-3 to C-1) sub-units. This is also consistent with the field observation that there is no time break/erosional unconformity or paleosol between the three investigated fall units.

Proximal fall deposits preserved on the crater rim are dominated by bimodal compositions whereas distal tephras record a full range of geochemical heterogeneity. The presence of intermediate glass compositions in the distal tephras, not currently observed in the proximal records, clearly evidences the interaction of two

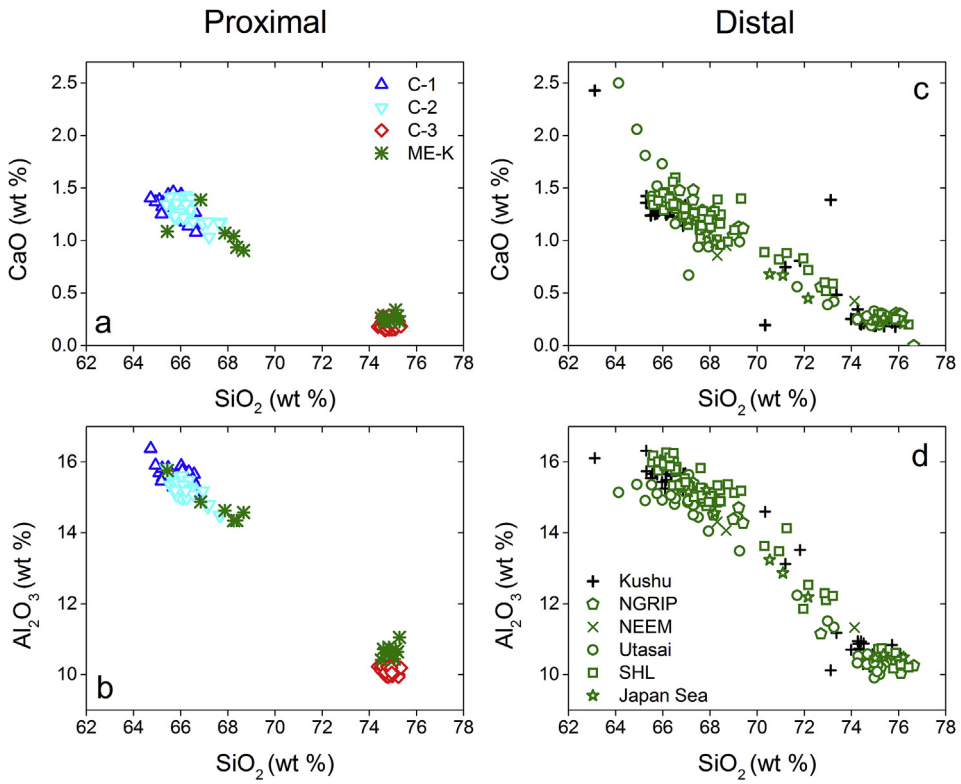

Fig. 10. Major element variation diagrams showing the glass compositions of (a–b) proximal tephra deposits in both Chinese (this study) and N. Korean ME sequences; (c–d) distal ME tephra deposits found in northeast China, Sea of Japan, Hokkaido and Greenland. ME-K represents the proximal ME sequence in N. Korean side of the crater (Sun et al., 2014a). Kushu represents the Lake Kushu on Rebun Island, Hokkaido, Japan (this study). Utasai represents the Utasai Bog in Hokkaido, Japan (Hughes et al., 2013). SHL represents the Sihailongwan Lake in northeast China (Sun et al., 2015). Japan Sea represents the distal ME tephra deposits found in Sea of Japan marine cores (Machida et al., 1990). NGRIP and NEEM represent the ultra-distal ME tephra deposits found in Greenland ice cores (Coulter et al., 2012; Sun et al., 2014a).

compositionally distinct magma batches during the caldera forming eruption. Moreover, the interaction of the two magma batches was not substantial otherwise this would be reflected in the proximal record with evidence of mingling in the pumices. In fact, there is no such evidence in our pumice samples. Overall, the observed compositional diversity indicates that the trachytic and rhyolitic magmas were not thoroughly mixed so only a minor portion of intermediate compositions were generated during magmatic interaction, which were then transferred into the stratosphere during the syn-eruptive process and were consequently recorded in the distal realms.

The preservation of bimodal proximal deposits (comprising the least and most fractionated components) has been reported from calderas elsewhere including in Afro-Arabia (Ukstins Peate et al., 2003; Ukstins Peate et al., 2008). As reported herein, the proximal units in Arabia are markedly bimodal and contrast with the contemporaneous distal tephra layers from 3000 km away in the Indian Ocean. These distal tephras display a continuum of compositions with end-members identical to the bimodal end-members found proximally. The bias between proximal and distal magma sequences is controversial and may relate to high level sub-volcanic processes that include fractionation processes involving silica rich magmas (Grove and Donnelly-Nolan, 1986), large scale liquid immiscibility (Charlier et al., 2011) and/or melt-crystal dynamics (Dufek and Bachmann, 2010).

7.2. Bayesian age modelling for Kushu tephra

The ME tephra deposits have been dated either directly or indirectly by multiple methods in many localities over the past two decades (Table 1). The proximal ages are mainly derived from the indirect dating method of ^{14}C dating of charcoals preserved in the pyroclastic fall and flow deposits (e.g. Horn and Schmincke, 2000; Nakamura et al., 2007; Yatsuzuka et al., 2010; Yin et al., 2012; Xu et al., 2013). Besides, direct dating of primary minerals using U-series TIMS (Wang et al., 2001) and $^{40}Ar/^{39}Ar$ (Yang et al., 2014) methods has also provided additional age constraints on the eruption. Distally, B–Tm tephra deposits were found in varve lakes in Japan and northeast China where the eruption was dated by varve chronology (Fukusawa et al., 1998; Kamite et al., 2010; Sun et al., 2015). Ultra-distal B–Tm tephra deposits were reported from the Greenland ice cores and as such the eruption has ages derived from the GICC05 and GISP2 ice-core chronologies (Sun et al., 2014a). Most recently, Sigl et al. (2015) has proposed a slight revision to the GICC05 chronology for the past 2500 years. This new NS1-2011 chronology, based on ^{10}Be and ^{14}C synchronization of ice-core and tree-ring timescales, has shifted the age of the ME from AD 941 ± 1 (GICC05) to AD 946–947 (Sigl et al., 2015).

In order to test our chemical correlation of the Kushu tephra to the proximal units and distal B–Tm, we have constructed a formal Bayesian age model for the late Holocene radiocarbon ages in the Kushu core (Fig. 11), for comparison with the highest resolution distal age reported for this tephra. In this age model, we have modelled the AMS ^{14}C dates reported in Müller et al. (in press), for Kushu along with the depth information (Table 3) in a Bayesian *P_Sequence* model with the addition of sediment deposition modelling to calculate the highest likelihood age ranges for every 1.6 cm, incorporating formal outlier detection (Bronk Ramsey, 2009a, b; 2013), applying the IntCal13 calibration curve (Reimer et al., 2013). As there are no radiocarbon dates in the same

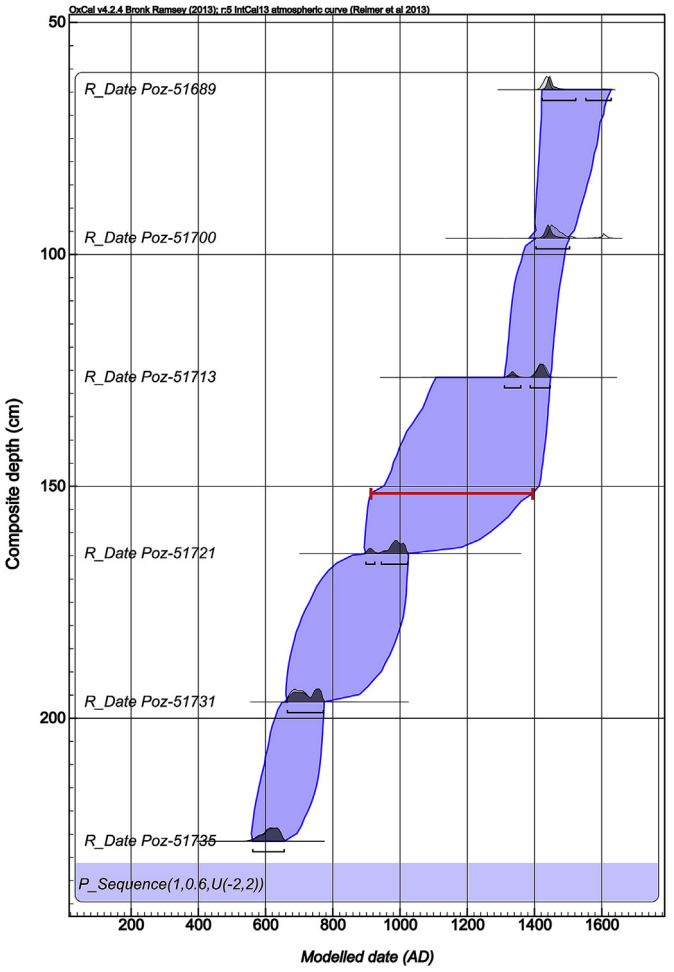

Fig. 11. 95% confidence Highest Probability Density output for radiocarbon-based Bayesian age-depth model for the uppermost 2 m sequence of Lake Kushu (run using a Poisson process model). The model was constructed purely using AMS ^{14}C dates of Kushu sediments from Müller et al. (in press), for providing independent age constraint on the Kushu tephra. The deposition model age range for the depth of 151.5 cm, which is the average position for the initial onset of the Kushu tephra, is 913–1395 cal AD.

centimeter of the core as the proposed B–Tm tephra, it was necessary to determine the age range for its depth at 151.5 cm, which is the average position in the core for the initial onset of Kushu tephra. The age range for the depth of 151.5 cm is 913–1395 cal AD (Fig. 11; supplementary material), and while at fairly low resolution this comfortably overlaps with the ice-core ages of the ME/B–Tm.

Due to the low resolution generated by the requirement to model the ages and associated uncertainty of the depths between the radiocarbon ages in this approach we also attempted to test the chronological relationship between the Kushu tephra and the high resolution age for the B–Tm in more detail. The logic of the test is that, while the radiocarbon ages for the Kushu site (Fig. 11) show a broadly last millennium age for the tephra sitting at 151 cm, if our correlation is correct then the tephra and radiocarbon ages should all be compatible with a high precision age model. We have thus constructed two more constrained age models (Fig. 12). We again use the above radiocarbon ages and their depths (Table 3), without interpolation and have also imported the GICC05 (Sun et al., 2014a, Fig. 12a) and NS1-2011 (Sigl et al., 2015, Fig. 12b) ages for the ME/B–Tm at the depth of our proposed correlative tephra in Kushu. We have applied a *P_Sequence* depositional model in Oxcal (Bronk Ramsey, 2013), with a variable K factor and automatic outlier detection, following Bronk Ramsey (2008; 2009a, b) with boundaries at the top and bottom of the selected 2 m sequence. The outlier model selection used the general outlier model and outlier probabilities were set to 0.05%. The results of the modelling exercise are reported as 95% confidence highest probability density function and depositional model plots. In these higher resolution, more constrained models, we are testing if the B–Tm ages are fully consistent with the Kushu radiocarbon ages and the depths in the core in which they sit. If our data is incompatible with the B–Tm on chronological grounds we would expect that the B–Tm ages we have incorporated, or the radiocarbon ages above and below the tephra would be reported as being anomalous by the outlier detection software. In these cases, however only the uppermost date Poz-51689 reported significant potential to be an outlier and thus the weighting of this date was reduced automatically in each age model. The dates close to the tephra layer, were, however, in reasonable agreement with the imported tephra ages. The two final modelled ages associated with GICC05 and NS1-2011 timescales, taking into account the depth and all chronological information are 933–949 and 944–947 cal AD (95.4%), respectively (Fig. 12; Table 3). We, thus, suggest on this rigorous basis, using formal deposition models the Kushu tephra is both chemically and chronologically well correlated to the ME/B–Tm.

7.3. Implication for future studies

High-resolution (annual to decadal-scale) reconstructions of past environments, and better understanding which role

Table 3
Summary of radiocarbon dates from Kushu sediments and ice-core ages for B–Tm that were used to construct the Bayesian age-depth models, the modelled date results shown in 95% confidence, and the relative depth information. AMS ^{14}C uncal. dates are from Müller et al. (in press). Date shown in italic font may be an age inversion although after calibration this still contributes significant probability to the deposition model. GICC05 ice-core tephra age for the B–Tm is from Sun et al. (2014a), the revised B–Tm age based on NS1-2011 timescale is from Sigl et al. (2015). The Bayesian age-depth models are produced using OxCal v4.2.4 (Bronk Ramsey, 2013). The modelled date results for the set of 6 AMS-dated samples are from the model with GICC05 tephra age imported as shown in Fig. 12a.

Laboratory number	Composite depth	AMS ^{14}C date	Modelled date (OxCal v4.2.4), 95% range			
	cm	uncal. yr BP	From, cal. BP	To, cal. BP	From, cal. AD	To, cal. AD
Poz-51689	*64.5*	*470 ± 25*	528	325	1422	1626
Poz-51700	96.5	415 ± 30	569	449	1381	1502
Poz-51713	126.5	510 ± 35	653	500	1297	1450
Poz-51721	164.5	1065 ± 25	1055	1004	895	947
Poz-51731	196.5	1290 ± 30	1285	1180	666	771
Poz-51735	226.5	1445 ± 30	1386	1296	565	655
Imported tephra	Imported position	Imported ice-core ages				
B–Tm	151	AD 941 ± 1 (GICC05 timescale)	1017	1001	933	949
		AD 946–947 (NS1-2011 timescale)	1006	1003	944	947

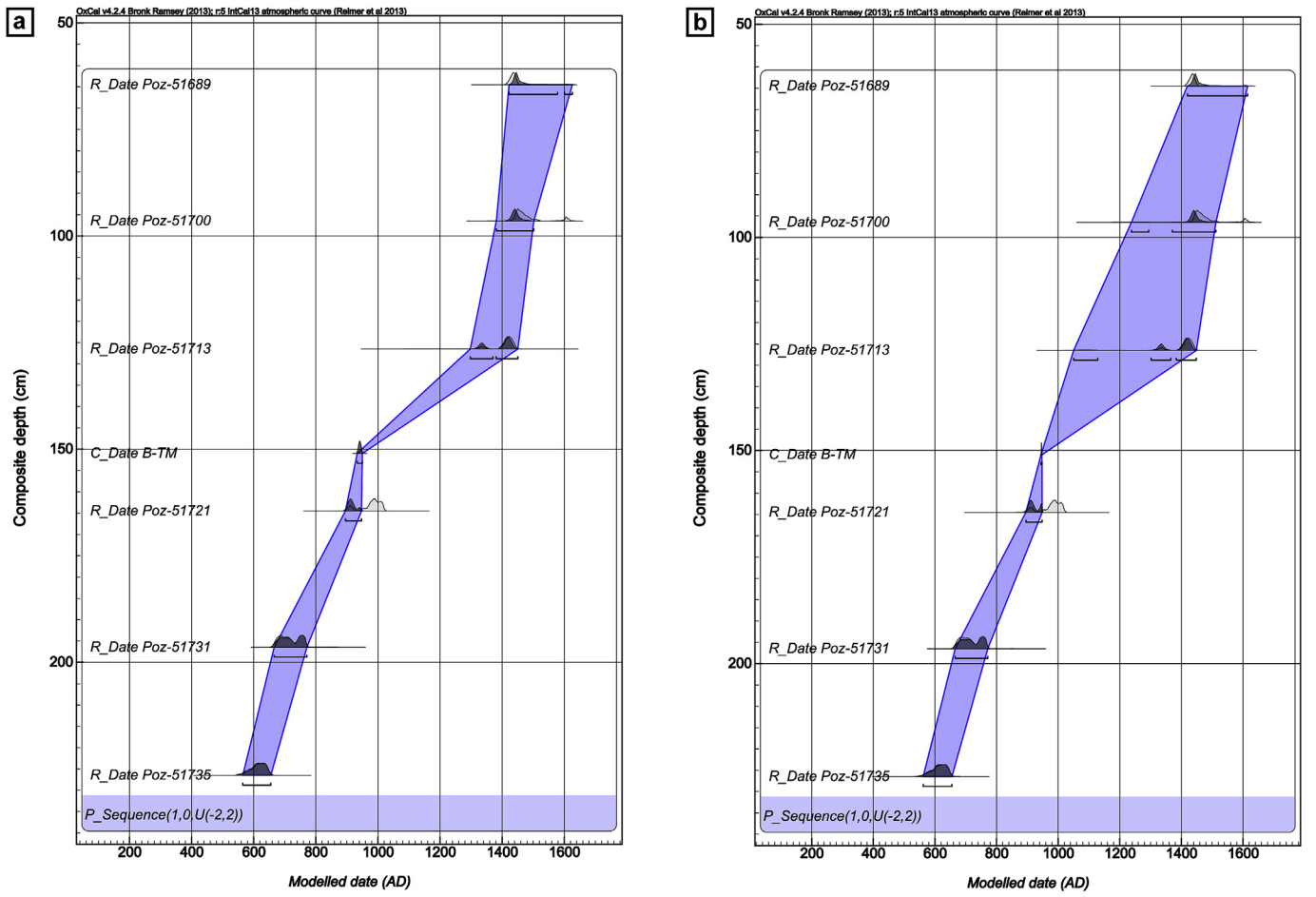

Fig. 12. (a) 95% confidence Highest Probability Density output for Bayesian age-depth model for the uppermost 2 m sequence of Lake Kushu (run using a Poisson process model). The model was constructed using the AMS ^{14}C dates reported in Müller et al. (in press) and the GICC05 ice-core age for B–Tm tephra (Sun et al., 2014a) imported in the appropriate position where our proposed correlative tephra was identified; (b) As above but with the B–Tm age from the revised NS1-2011 timescale after Sigl et al. (2015).

environmental and climatic changes played in the cultural dynamics remains extremely important, though an empirically challenging question for the Hokkaido region (Weber et al., 2013). Despite, the northern part of Japan, including Hokkaido and adjacent islands are rich in archaeological and environmental archives, the main challenge remains the scarcity of published records with high temporal resolution and adequate dating control (Nakagawa et al., 2012; Müller et al., in press and references therein). These two common problems hinder direct correlation between individual archives, thus preventing inter-regional comparison and identification of leads and lags in reconstructed climate variability. A multidisciplinary research on the RK12 core from Lake Kushu started in 2012 has a significant potential to fill the existing gap in the current knowledge and to build up the high-resolution environmental archive spanning the past ca. 17,000 years (Müller et al., in press). However, in order to serve as a link between the high-resolution and accurately-dated records from central Japan (e.g. Lake Suigetsu: Nakagawa et al., 2012), China (e.g. Sihailongwan Maar Lake: Stebich et al., 2009, 2015), and North Atlantic region, the Kushu ^{14}C chronology must be checked, and when necessary, improved. The current study demonstrates the potential of cryptotephra analysis for improving the age constraints on the Kushu sedimentary record. The ice-core ages imported into the deposition models significantly help constrain the age of the sediments around the tephra layer and improve the radiocarbon chronology in this interval (Fig. 12). This provides encouragement for the identification of additional cryptotephra layers in the Lake Kushu sediment. Though it still could be improved, we believe that the existing RK12 core chronology based on the 57 AMS dates (Müller et al., in press) is robust enough to provide reliable age estimations for the tephra layers preserved in the sediment. This will facilitate search of the source volcano and identification of the eruption, which produced each given tephra.

8. Conclusions

a) Three proximal pyroclastic fall units (i.e. C-3 to C-1) from Tianwen summit on the crater rim of Changbaishan Volcano, NE China display bimodal glass compositions comprising trachyte and rhyolite end-member compositions.
b) A distal tephra layer in Lake Kushu of northern Japan contains glass shards that define a complete compositional continuum ranging from trachyte to rhyolite that in themselves are chemically identical to the investigated proximal glasses.
c) The chemical constraint and radiocarbon-based Bayesian age-depth model indicate that the analysed Kushu tephra is the distal expression of the Millennium eruption.
d) Proximal-distal geochemical correlation at a full spectrum of element level (i.e. major, minor and trace elements) requires that the three proximal pyroclastic fall units were erupted as

part of the Millennium eruption as alluded to by previous studies (Horn and Schmincke, 2000; Sun et al., 2014a).

e) Bayesian age-depth modelling of Kushu sediments involving the AMS ^{14}C dates and two ice-core derived ages for the B–Tm provides 95% confidence interval ranges of 933–949 and 944–947 cal AD for the Kushu tephra. The high resolution ice-core tephra ages imported into the deposition models help test and ultimately constrain the radiocarbon chronology in this interval of the Lake Kushu sedimentary record.

f) The presence of intermediate glass compositions in the distal tephra layers, not currently observed in the proximal records, clearly evidences the interaction of two compositionally distinct magma batches (with end-member compositions) during the caldera forming eruption.

Acknowledgements

This study was supported by the External Cooperation Program of Bureau of International Co-operation, Chinese Academy of Sciences, Grant No. 132744KYSB20130005. XYC's stay at RHUL was supported by the collaboration scheme between GIGCAS and RHUL. Coring of Lake Kushu and core transportation costs were covered by the Japanese MEXT-Japan Kakenhi research grant No. 21101002 held by Dr. H. Yonenobu, whose generous help we greatly acknowledge. The Baikal–Hokkaido Archaeology Project and BHAP-related research activities on Rebun Island are supported by the Major Collaborative Research Initiative (MCRI) program of the Social Sciences and Humanities Research Council of Canada, and collaborating institutions, including University of Alberta, German Archaeological Institute (DAI), Free University Berlin and German Science Foundation (DFG TA 540/5), Hokkaido University, and Japan Society for the Promotion of Science. We would like to thank Prof. F. Wang for providing proximal tephra sub-samples; Dr. C. J. Manning for the assistance in sample preparation; Dr. S. Armitage for beneficial discussions; Dr. V. C. Smith and an anonymous reviewer for their detailed and constructive feedback. We thank N. Holloway for preparing samples in epoxy resin stubs; K. Flowers and S. Gibbons for their assistance in the lab.

Appendix A. Supplementary data

Supplementary data related to this article can be found at http://dx.doi.org/10.1016/j.quageo.2016.02.003.

References

Albert, P.G., Hardiman, M., Keller, J., Tomlinson, E.L., Smith, V.C., Bourne, A.J., Wulf, S., Zanchetta, G., Sulpizio, R., Müller, U.C., Pross, J., Ottolini, L., Matthews, I.P., Blockley, S.P.E., Menzies, M.A., 2015. Revisiting the Y-3 tephrostratigraphic marker: a new diagnostic glass geochemistry, age estimate, and details on its climatostratigraphical context. Quat. Sci. Rev. 118, 105–121.

Albert, P.G., Tomlinson, E.L., Lane, C.S., Wulf, S., Smith, V.C., Coltelli, M., Keller, J., Lo Castro, D., Manning, C.J., Müller, W., Menzies, M.A., 2013. Late glacial explosive activity on Mount Etna: Implications for proximal–distal tephra correlations and the synchronisation of Mediterranean archives. J. Volcanol. Geotherm. Res. 265 (0), 9–26.

Albert, P.G., Tomlinson, E.L., Smith, V.C., Di Roberto, A., Todman, A., Rosi, M., Marani, M., Muller, W., Menzies, M.A., 2012. Marine-continental tephra correlations: volcanic glass geochemistry from the Marsili Basin and the Aeolian Islands, Southern Tyrrhenian Sea, Italy. J. Volcanol. Geotherm. Res. 229–230, 74–94.

Allan, A.S.R., Baker, J.A., Carter, L., Wysoczanksi, R.J., 2008. Reconstructing the quaternary evolution of the world's most active silicic volcanic system: insights from an ~1.65 Ma deep ocean tephra record sourced from Taupo Volcanic Zone, New Zealand. Quat. Sci. Rev. 27 (25–26), 2341–2360.

Blockley, S.P.E., Pyne-O'Donnell, S.D.F., Lowe, J.J., Matthews, I.P., Stone, A., Pollard, A.M., Turney, C.S.M., Molyneux, E.G., 2005. A new and less destructive laboratory procedure for the physical separation of distal glass tephra shards from sediments. Quat. Sci. Rev. 24 (16–17), 1952–1960.

Bronk Ramsey, C., 2008. Deposition models for chronological records. Quat. Sci. Rev. 27 (1–2), 42–60.

Bronk Ramsey, C., 2009a. Bayesian analysis of radiocarbon dates. Radiocarbon 51 (1), 337–360.

Bronk Ramsey, C., 2009b. Dealing with outliers and offsets in radiocarbon dating. Radiocarbon 51 (3), 1023–1045.

Bronk Ramsey, C., 2013. OxCal 4.2. Available from: http://c14.arch.ox.ac.uk/oxcal.

Charlier, B., Namur, O., Toplis, M.J., Schiano, P., Cluzel, N., Higgins, M.D., Auwera, J.V., 2011. Large-scale silicate liquid immiscibility during differentiation of tholeiitic basalt to granite and the origin of the daly gap. Geology 39 (10), 907–910.

Chen, X.Y., Xu, Y.G., Menzies, M., 2014. Tephrochronology: principles and applications. Acta Petrol. Sin. 30 (12), 3491–3500 (in Chinese with English abstract).

Coulter, S.E., Pilcher, J.R., Plunkett, G., Baillie, M., Hall, V.A., Steffensen, J.P., Vinther, B.M., Clausen, H.B., Johnsen, S.J., 2012. Holocene tephras highlight complexity of volcanic signals in Greenland ice cores. J. Geophys. Res. Atmos. 117, D21303.

Cui, Z., Wei, H., Liu, R., 1995. Historical documentation research of eruptions of the Tianchi Volcano, Changbaishan. In: Liu, R. (Ed.), Volcanism and Human Environment. Seismology Press, Beijing, pp. 36–39 (in Chinese).

Dufek, J., Bachmann, O., 2010. Quantum magmatism: magmatic compositional gaps generated by melt-crystal dynamics. Geology 38 (8), 687–690.

Fan, Q., Liu, R., Wei, H., Sui, J., Li, N., 1999. Petrogeochemical characteristics of holocene eruption of the Tianchi Volcano, Changbai Mountains. Geol. Rev. 45 (Sup.), 263–271 (in Chinese with English abstract).

Fukusawa, H., Tsukamoto, S., Tsukamoto, H., Ikeda, M., Okamura, M., MAtsuoka, H., 1998. Falling age of Baegdusan-Tomakomai tephra (B-Tm) estimated by using non-glacial varves. Laguna 5, 55–62 (in Japanese with English abstract).

Furuta, T., Fujioka, K., Arai, F., 1986. Widespread submarine tephras around Japan — petrographic and chemical properties. Mar. Geol. 72 (1), 125–142.

Grove, T.L., Donnelly-Nolan, J.M., 1986. The evolution of young silicic lavas at Medicine Lake Volcano, California: implications for the origin of compositional gaps in calc-alkaline series lavas. Contrib. Mineral. Pet. 92 (3), 281–302.

Guo, Z., Liu, J., Sui, S., Liu, Q., He, H., Ni, Y., 2002. The mass estimation of volatile emission during 1199–1200 AD eruption of Baitoushan volcano and its significance. Sci. China Ser. D Earth Sci. 45 (6), 530–539.

Horn, S., Schmincke, H.-U., 2000. Volatile emission during the eruption of Baitoushan Volcano (China/North Korea) ca. 969 AD. Bull. Volcanol. 61 (8), 537–555.

Hughes, P.D.M., Mallon, G., Brown, A., Essex, H.J., Stanford, J.D., Hotes, S., 2013. The impact of high tephra loading on late-Holocene carbon accumulation and vegetation succession in peatland communities. Quat. Sci. Rev. 67 (0), 160–175.

Irvine, T.N., Baragar, W.R.A., 1971. A guide to the chemical classification of the common volcanic rocks. Can. J. Earth Sci. 8 (5), 523–548.

Ji, F., Li, J., Zheng, R., 1999. The preliminary study of TL chronology for recent eruptive materials in Changbaishan Tianchi Volcano. Geol. Rev. 45 (Sup.), 282–286 (in Chinese with English abstract).

Jochum, K.P., Stoll, B., Herwig, K., Willbold, M., Hofmann, A.W., Amini, M., Aarburg, S., Abouchami, W., Hellebrand, E., Mocek, B., Raczek, I., Stracke, A., Alard, O., Bouman, C., Becker, S., Dücking, M., Brätz, H., Klemd, R., de Bruin, D., Canil, D., Cornell, D., de Hoog, C.-J., Dalpé, C., Danyushevsky, L., Eisenhauer, A., Gao, Y., Snow, J.E., Groschopf, N., Günther, D., Latkoczy, C., Guillong, M., Hauri, E.H., Höfer, H.E., Lahaye, Y., Horz, K., Jacob, D.E., Kasemann, S.A., Kent, A.J.R., Ludwig, T., Zack, T., Mason, P.R.D., Meixner, A., Rosner, M., Misawa, K., Nash, B.P., Pfänder, J., Premo, W.R., Sun, W.D., Tiepolo, M., Vannucci, R., Vennemann, T., Wayne, D., Woodhead, J.D., 2006. MPI-DING reference glasses for in situ microanalysis: new reference values for element concentrations and isotope ratios. Geochem. Geophys. Geosystems 7 (2), Q02008.

Kamite, M., Yamada, K., Saito-Kato, M., Okuno, M., Yasuda, Y., 2010. Microscopic observations of varve sediments from Lake Ni-no-Megata and Lake San-no-Megata, Oga Peninsula, NE Japan, with reference to the fallout age of the B-Tm Tephra. Jour. Geol. Soc. Jpn. 116 (7), 349–359 (in Japanese with English abstract).

Kumano, S., Ihira, M., Kuromi, M., Maeda, Y., Matsumoto, E., Nakamura, T., Matsushima, Y., Sato, H., Matsuda, I., 1990. Holocene sedimentary history of some coastal plains in Hokkaido, Japan V. Sedimentary history of Kushu Lake and Akkeshi. Ecol. Res. 5 (3), 277–289.

Kyle, P.R., Ponomareva, V.V., Rourke Schluep, R., 2011. Geochemical characterization of marker tephra layers from major Holocene eruptions, Kamchatka Peninsula, Russia. Int. Geol. Rev. 53 (9), 1059–1097.

Lane, C.S., Blockley, S.P.E., Mangerud, J., Smith, V.C., Lohne, Ø.S., Tomlinson, E.L., Matthews, I.P., Lotter, A.F., 2012. Was the 12.1 ka Icelandic Vedde ash one of a kind? Quat. Sci. Rev. 33 (0), 87–99.

Lane, C.S., Brauer, A., Martín-Puertas, C., Blockley, S.P.E., Smith, V.C., Tomlinson, E.L., 2015. The Late Quaternary tephrostratigraphy of annually laminated sediments from Meerfelder Maar, Germany. Quat. Sci. Rev. 122, 192–206.

Le Bas, M.J., Le Maitre, R.W., Streckeisen, A., Zanettin, B., 1986. A chemical classification of volcanic rocks based on the total alkali-silica diagram. J. Petrol. 27 (3), 745–750.

Liu, R., Fan, Q., Wei, H., Li, N., 1999. Study on active volcanoes of China. Geol. Rev. 45 (Sup.), 3–15 (in Chinese with English abstract).

Liu, R., Wei, H., Li, J., 1998. The Latest Eruptions from Tianchi Volcano, Changbaishan. SciencePress, Beijing (in Chinese).

MacDonald, R., 1974. Nomenclature and petrochemistry of the peralkaline oversaturated extrusive rocks. Bull. Volcanol. 38 (2), 498–516.

Machida, H., Arai, F., 1983. Extensive ash falls in and around the sea of Japan from large late quaternary eruptions. J. Volcanol. Geotherm. Res. 18 (1–4), 151–164.
Machida, H., Moriwaki, H., Zhao, D.-C., 1990. The recent major eruption of Changbai Volcano and its environmental effects. Geogr. Rep. Tokyo Metrop. Univ. 25, 1–20.
MacLeod, A., Matthews, I.P., Lowe, J.J., Palmer, A.P., Albert, P.G., 2015. A second tephra isochron for the Younger Dryas period in northern Europe: the Abernethy Tephra. Quat. Geochronol. 28, 1–11.
Müller, S., Schmidt, M., Kossler, A., Leipe, C., Irino, T., Yamamoto, M., Yonenobu, H., Goslar, T., Kato, H., Wagner, M., Weber, A.W., Tarasov, P.E., 2016. Palaeobotanical records from Rebun Island and their potential for improving the chronological control and understanding human-environment interactions in the Hokkaido Region, Japan. Holocene (in press).
Nakagawa, T., Gotanda, K., Haraguchi, T., Danhara, T., Yonenobu, H., Brauer, A., Yokoyama, Y., Tada, R., Takemura, K., Staff, R.A., Payne, R., Bronk Ramsey, C., Bryant, C., Brock, F., Schlolaut, G., Marshall, M., Tarasov, P., Lamb, H., 2012. SG06, a fully continuous and varved sediment core from Lake Suigetsu, Japan: stratigraphy and potential for improving the radiocarbon calibration model and understanding of late Quaternary climate changes. Quat. Sci. Rev. 36, 164–176.
Nakamura, T., Okuno, M., Kimura, K., Mitsutani, T., Moriwaki, H., Ishizuka, Y., Kim, K.H., Jing, B.L., Oda, H., Minami, M., Takada, H., 2007. Application of 14C wiggle-matching to support dendrochronological analysis in Japan. Tree-Ring Res. 63 (1), 37–46.
Nanayama, F., Satake, K., Furukawa, R., Shimokawa, K., Atwater, B.F., Shigeno, K., Yamaki, S., 2003. Unusually large earthquakes inferred from tsunami deposits along the Kuril trench. Nature 424 (6949), 660–663.
Okuno, M., Torii, M., Yamada, K., Shinozuka, Y., Danhara, T., Gotanda, K., Yonenobu, H., Yasuda, Y., 2011. Widespread tephras in sediments from lake Ichino-Megata in northern Japan: their description, correlation and significance. Quat. Int. 246 (1–2), 270–277.
Reimer, P.J., Bard, E., Bayliss, A., Beck, J.W., Blackwell, P.G., Bronk Ramsey, C., Buck, C.E., Cheng, H., Edwards, R.L., Friedrich, M., Grootes, P.M., Guilderson, T.P., Haflidason, H., Hajdas, I., Hatté, C., Heaton, T.J., Hoffmann, D.L., Hogg, A.G., Hughen, K.A., Kaiser, K.F., Kromer, B., Manning, S.W., Niu, M., Reimer, R.W., Richards, D.A., Scott, E.M., Southon, J.R., Staff, R.A., Turney, C.S.M., van der Plicht, J., 2013. IntCal13 and Marine13 radiocarbon age calibration curves 0–50,000 Years cal BP. Radiocarbon 55 (4), 1869–1887.
Sigl, M., Winstrup, M., McConnell, J.R., Welten, K.C., Plunkett, G., Ludlow, F., Buntgen, U., Caffee, M., Chellman, N., Dahl-Jensen, D., Fischer, H., Kipfstuhl, S., Kostick, C., Maselli, O.J., Mekhaldi, F., Mulvaney, R., Muscheler, R., Pasteris, D.R., Pilcher, J.R., Salzer, M., Schupbach, S., Steffensen, J.P., Vinther, B.M., Woodruff, T.E., 2015. Timing and climate forcing of volcanic eruptions for the past 2,500 years. Nature 523 (7562), 543–549.
Smith, V.C., Isaia, R., Pearce, N.J.G., 2011a. Tephrostratigraphy and glass compositions of post-15 kyr Campi Flegrei eruptions: implications for eruption history and chronostratigraphic markers. Quat. Sci. Rev. 30 (25–26), 3638–3660.
Smith, V.C., Mark, D.F., Staff, R.A., Blockley, S.P.E., Ramsey, C.B., Bryant, C.L., Nakagawa, T., Han, K.K., Weh, A., Takemura, K., Danhara, T., 2011b. Toward establishing precise 40Ar/39Ar chronologies for Late Pleistocene palaeoclimate archives: an example from the Lake Suigetsu (Japan) sedimentary record. Quat. Sci. Rev. 30 (21–22), 2845–2850.
Smith, V.C., Pearce, N.J.G., Matthews, N.E., Westgate, J.A., Petraglia, M.D., Haslam, M., Lane, C.S., Korisettar, R., Pal, J.N., 2011c. Geochemical fingerprinting of the widespread Toba tephra using biotite compositions. Quat. Int. 246 (1–2), 97–104.
Smith, V.C., Staff, R.A., Blockley, S.P.E., Bronk Ramsey, C., Nakagawa, T., Mark, D.F., Takemura, K., Danhara, T., 2013. Identification and correlation of visible tephras in the Lake Suigetsu SG06 sedimentary archive, Japan: chronostratigraphic markers for synchronising of east Asian/west Pacific palaeoclimatic records across the last 150 ka. Quat. Sci. Rev. 67 (0), 121–137.
Stebich, M., Mingram, J., Han, J., Liu, J., 2009. Late Pleistocene spread of (cool-) temperate forests in Northeast China and climate changes synchronous with the North Atlantic region. Glob. Planet. Change 65 (1–2), 56–70.
Stebich, M., Rehfeld, K., Schlütz, F., Tarasov, P.E., Liu, J., Mingram, J., 2015. Holocene vegetation and climate dynamics of NE China based on the pollen record from Sihailongwan Maar Lake. Quat. Sci. Rev. 124, 275–289.
Sun, C., Plunkett, G., Liu, J., Zhao, H., Sigl, M., McConnell, J.R., Pilcher, J.R., Vinther, B., Steffensen, J.P., Hall, V., 2014a. Ash from Changbaishan Millennium eruption recorded in Greenland ice: implications for determining the eruption's timing and impact. Geophys. Res. Lett. 2013, GL058642.
Sun, C., You, H., He, H., Zhang, L., Gao, J., Guo, W., Chen, S., Mao, Q., Liu, Q., Chu, G., Liu, J., 2015. New evidence for the presence of Changbaishan Millennium eruption ash in the Longgang volcanic field. Northeast China. Gondwana Res. 28 (1), 52–60.
Sun, C.Q., You, H.T., Liu, J.Q., Li, X., Gao, J.L., Chen, S.S., 2014b. Distribution, geochemistry and age of the Millennium eruptives of Changbaishan Volcano, Northeast China - a review. Front. Earth Sci. 8 (2), 216–230.
Sun, S.-s., McDonough, W.F., 1989. Chemical and isotopic systematics of oceanic basalts: implications for mantle composition and processes. Geol. Soc. Lond. Spec. Publ. 42 (1), 313–345.
Tomlinson, E.L., Albert, P.G., Wulf, S., Brown, R.J., Smith, V.C., Keller, J., Orsi, G., Bourne, A.J., Menzies, M.A., 2014. Age and geochemistry of tephra layers from Ischia, Italy: constraints from proximal-distal correlations with Lago Grande di Monticchio. J. Volcanol. Geotherm. Res. 287, 22–39.
Tomlinson, E.L., Arienzo, I., Civetta, L., Wulf, S., Smith, V.C., Hardiman, M., Lane, C.S., Carandente, A., Orsi, G., Rosi, M., Müller, W., Menzies, M.A., 2012. Geochemistry of the Phlegraean Fields (Italy) proximal sources for major Mediterranean tephras: implications for the dispersal of Plinian and co-ignimbritic components of explosive eruptions. Geochim. Cosmochim. Acta 93 (0), 102–128.
Tomlinson, E.L., Smith, V.C., Albert, P.G., Aydar, E., Civetta, L., Cioni, R., Cubukcu, E., Gertisser, R., Isaia, R., Menzies, M.A., Orsi, G., Rosi, M., Zanchetta, G., 2015. The major and trace element glass compositions of the productive Mediterranean volcanic sources: tools for correlating distal tephra layers in and around Europe. Quat. Sci. Rev. 118, 48–66.
Tomlinson, E.L., Thordarson, T., Müller, W., Thirlwall, M., Menzies, M.A., 2010. Microanalysis of tephra by LA-ICP-MS — Strategies, advantages and limitations assessed using the Thorsmörk ignimbrite (Southern Iceland). Chem. Geol. 279 (3–4), 73–89.
Ukstins Peate, I., Baker, J.A., Kent, A.J.R., Al-Kadasi, M., Al-Subbary, A., Ayalew, D., Menzies, M., 2003. Correlation of Indian Ocean tephra to individual Oligocene silicic eruptions from Afro-Arabian flood volcanism. Earth Planet. Sci. Lett. 211 (3–4), 311–327.
Ukstins Peate, I., Kent, A.J.R., Baker, J.A., Menzies, M.A., 2008. Extreme geochemical heterogeneity in Afro-Arabian Oligocene tephras: preserving fractional crystallization and mafic recharge processes in silicic magma chambers. Lithos 102 (1–2), 260–278.
Wang, F., Chen, W.-j., Peng, Z.-c., Li, Q., 2001. Activity of Cangbaishan Tianchi Volcano since late Pleistocene: the constrain from geochronology of high precision U-series TIMS method. Geochimica 30 (1), 88–94 (in Chinese with English abstract).
Weber, A.W., Jordan, P., Kato, H., 2013. Environmental change and cultural dynamics of Holocene hunter–gatherers in Northeast Asia: comparative analyses and research potentials in Cis-Baikal (Siberia, Russia) and Hokkaido (Japan). Quat. Int. 290–291, 3–20.
Wei, H., Liu, G., Gill, J., 2013. Review of eruptive activity at Tianchi volcano, Changbaishan, northeast China: implications for possible future eruptions. Bull. Volcanol. 75 (4), 1–14.
Wei, H., Wang, Y., Jin, J., Gao, L., Yun, S.-H., Jin, B., 2007. Timescale and evolution of the intracontinental Tianchi volcanic shield and ignimbrite-forming eruption, Changbaishan, Northeast China. Lithos 96 (1–2), 315–324.
Xu, J., Pan, B., Liu, T., Hajdas, I., Zhao, B., Yu, H., Liu, R., Zhao, P., 2013. Climatic impact of the millennium eruption of Changbaishan volcano in China: new insights from high-precision radiocarbon wiggle-match dating. Geophys. Res. Lett. 40 (1), 54–59.
Yang, L., Wang, F., Feng, H., Wu, L., Shi, W., 2014. 40Ar/39Ar geochronology of Holocene volcanic activity at Changbaishan Tianchi volcano, Northeast China. Quat. Geochronol. 21, 106–114.
Yatsuzuka, S., Okuno, M., Nakamura, T., Kimura, K., Setoma, Y., Miyamoto, T., Kim, K.H., Moriwaki, H., Nagase, T., Jin, X., 2010. 14C wiggle-matching of the B-Tm tephra, Baitoushan volcano, China/North Korea. Radiocarbon 52 (3), 933–940.
Yin, J., Jull, A.J.T., Burr, G.S., Zheng, Y., 2012. A wiggle-match age for the millennium eruption of Tianchi Volcano at Changbaishan, Northeastern China. Quat. Sci. Rev. 47 (0), 150–159.
Yu, H., Wu, J., Xu, J., Lin, C., Shi, L., Chen, X., 2012. Microstructural Characteristics of the holocene pumice erupted from Changbaishan Tianchi Volcano and their volcanological implications (Earth Science Edition). J. Jilin Univ. 42 (Suppl. 3), 132–144 (in Chinese with English abstract).